

SIMULATION OF PREVIEW CONTROLLED ACTIVE
SUSPENSION FOR CONVOY VEHICLES

MD. MUSTAFIZUR RAHMAN



Simulation of Preview Controlled Active Suspension for Convoy Vehicles

by

©Md. Mustafizur Rahman

A Thesis submitted to the School of Graduate Studies in partial fulfillment of the
requirements for the degree of

Master of Engineering

Faculty of Engineering and Applied Science

Memorial University of Newfoundland

May, 2012

St. John's

Newfoundland

Abstract

Designing a vehicle suspension that can give very good ride comfort along with crisp handling has been a subject for researchers for the last three decades. Research shows that active suspension can give superior performance over passive and semi-active suspension systems. Preview controlled active suspension can further improve the performance but faces the issue of sensing the road ahead of the vehicle. Previous applications of preview control have used look-ahead sensors mounted on the front bumper to measure terrain beneath. Such sensors are vulnerable, potentially confused by water, snow, or other soft obstacles; and offer a fixed preview time. For convoy vehicle applications, this thesis proposes using the overall response of the preceding vehicle(s) to generate preview controller information for follower vehicles. A robust observer is used to estimate the states of a quarter car vehicle model, from which road profile is estimated and passed on to the follower vehicle(s) to generate a preview function. The preview-active suspension, implemented in discrete time using a shift register approach to improve simulation time, reduces sprung mass acceleration and dynamic tire deflection peaks by more than 50% and 40% respectively. Terrain can change from one vehicle to the next if a loose obstacle is dislodged, or if the vehicle paths are sufficiently different so that one vehicle misses a discrete road event. The resulting spurious preview information can give suspension performance worse than that of a passive or conventional active system. In this thesis, each vehicle can

effectively estimate the road profile based on its own state trajectory. By comparing its own road estimate with the preview information, preview errors can be detected and suspension control quickly switched from preview to conventional active control to preserve performance improvements compared to passive suspensions. Benefits of preview control for variation in sensor noise and more complex vehicle models must also be studied. For that, an estimation accuracy analysis has been done to study the effect of sensor noise. A half car vehicle model is also developed and discrete optimal control law is implemented to show the performance improvements. A good overall performance improvement for both the front and rear wheel is observed from the simulation results.

Acknowledgements

I would like to express my endless gratitude to my supervisor Dr. Geoff Rideout for his persistent help and encouragement throughout the thesis work. Without his valuable guidance and encouragement this work would not have been possible.

I would also like to thank Keith J. Wakeham, Himadri Shastry, Taufiqur Rahman and M. Raju Hossain for their inspirational comments, help and support from time to time.

I gratefully thank all my friends and family for their inspirations.

Table of Contents

Abstract	ii
Acknowledgments	iv
Table of Contents	viii
List of Tables	ix
List of Figures	xv
Notation	xvi
1 Introduction	1
1.1 Vehicle suspension systems	1
1.2 Convoy vehicle preview control	3
1.3 Research objectives	4
1.4 Contribution	5
1.5 Thesis outline	6
2 Literature Review	7
2.1 Background	7
2.2 Literature review	9

2.3	Organization of the report	12
3	Vehicle Models and State Space Representation	14
3.1	Vehicle models	15
3.1.1	Quarter car model	15
3.1.1.1	State space representation of quarter car model	16
3.1.2	Half car model	17
3.1.2.1	State space representation of half car model	19
3.2	Vehicle parameters	21
4	Optimal Preview Control of Convoy Vehicle Suspension: Quarter Car Model	22
4.1	Development of optimal control law	23
4.2	Discretization of continuous system	26
4.3	Simulation results	29
4.3.1	Road holding weighting factors	30
4.3.2	Ride quality weighting factors	33
4.4	Effect of preview time	35
5	Observer Design	39
5.1	Observer design background	40
5.2	Development of the proposed observer	41
6	Robust Convoy Preview with Active/Preview Switching	49
6.1	Scenario 1: Presence of faulty sensors in lead vehicle	50
6.2	Scenario 2: Mid-convoy terrain changes	50
6.3	Scenario 3: Lag/lead in the preview information	53
6.3.1	Small time lag (0.005 sec)	53

6.3.2	Larger time lag (0.025 sec)	58
6.3.3	Small lead time (0.005 sec)	58
6.3.4	Larger lead time (0.025 sec)	64
6.4	Convoy preview control	64
6.5	Preview-active to active switching	67
6.6	Summary	69
7	Estimation Accuracy and Robustness of Observer for Actively Sus-	
	pending Vehicle	73
7.1	Motivation	74
7.2	System model	74
7.3	Road disturbance input	76
7.4	Observer	77
7.5	Sensitivity to measurement noise	79
7.6	Results	80
7.7	Conclusion and future works	81
8	Optimal Preview Control of Convoy Vehicle Suspension: Half Car	
	Model	84
8.1	Development of optimal control law	84
8.2	Discretization of Continuous System	88
8.3	Simulation results	91
	8.3.1 Road holding weighting factors	92
	8.3.2 Ride quality weighting factors	96
9	Conclusion	102
9.1	Summary	102
9.2	Future works	104

Bibliography	105
Appendices	109
A Optimal Regulator Gain and the Riccati Equation	110
B Half Car LQR Matrices	113
C Discretization of Preview Function (Shift-Register Approach)	118
D MATLAB Codes	121
E SIMULINK Models	136

List of Tables

3.1	Quarter car model parameters	21
3.2	Half car model parameters	21
4.1	Improvements in performance compared to passive system for road holding weighting factors	36
4.2	Improvements in performance compared to active system for road holding weighting factors	36
4.3	Improvements in performance compared to passive system for ride quality weighting factors	37
4.4	Improvements in performance compared to passive system for ride quality weighting factors	38
7.1	Measurement Noise Intensities for Simulation	79
7.2	Simulation Results for Deterministic Road	81

List of Figures

1.1	'The military have used convoys for thousands of years to transport troops and equipment during wartime. Convoys are usually groups of vehicles traveling together for increased protection and mutual support'[The Brigade photo, 2011/Patty].	3
1.2	Preview control of convoy vehicles with lead follower communication as in [12]	4
3.1	2-DOF quarter car model	16
3.2	Half car model	18
4.1	Lead-follower arrangement for convoy preview	23
4.2	Wheel displacement (z_u) for Passive, Active and Preview-active suspension system (Preview time 0.2 sec)	31
4.3	Sprung mass acceleration (\ddot{z}_s) for Passive, Active and Preview-active suspension system (Preview time 0.2 sec)	31
4.4	Tire deflection ($z_u - z_r$) for Passive, Active and Preview-active suspension system (Preview time 0.2 sec)	32
4.5	Suspension deflection ($z_s - z_u$) for Passive, Active and Preview-active suspension system (Preview time 0.2 sec)	32

4.6	Wheel displacement (z_u) for Passive, Active and Preview-active suspension system for ride comfort(Preview time 0.2 sec)	33
4.7	Sprung mass acceleration (\ddot{z}_s) for Passive, Active and Preview-active suspension system for ride comfort(Preview time 0.2 sec)	34
4.8	Tire deflection ($z_u - z_r$) for Passive, Active and Preview-active suspension system for ride comfort(Preview time 0.2 sec)	34
4.9	Suspension deflection ($z_s - z_u$) for Passive, Active and Preview-active suspension system for ride comfort(Preview time 0.2 sec)	35
5.1	Schematic representation of the proposed observer	43
5.2	Block diagram of the observer	44
5.3	Actual vs. Estimated Wheel displacement (z_u) with preview(0.2s)	45
5.4	Actual vs. Estimated Sprung mass acceleration (\ddot{z}_s) with preview(0.2s)	46
5.5	Actual vs. Estimated Tire deflection ($z_u - z_r$) with preview(0.2s)	46
5.6	Actual vs. Estimated Suspension deflection ($z_s - z_u$) with preview(0.2s)	47
5.7	Road observation for the designed observer for rounded pulse	47
5.8	Road observation for the designed observer for two consecutive bumps	48
6.1	Incorrect road information generated by lead vehicle	50
6.2	Ride quality (\ddot{z}_s) of follower vehicle using correct and erroneous preview information	51
6.3	Unprung mass deflection (z_u) of follower vehicle using correct and erroneous preview information	51
6.4	Suspension deflection ($z_s - z_u$) of follower vehicle using correct and erroneous preview information	52
6.5	Tire deflection ($z_u - z_r$) of follower vehicle using correct and erroneous preview information	52

6.6	Ride quality (\dot{z}_s) of follower vehicle due to spurious preview information (No actual bump)	53
6.7	Unprung mass deflection (z_u) of follower vehicle due to spurious preview information (No actual bump)	54
6.8	Suspension deflection ($z_s - z_u$) of follower vehicle due to spurious preview information (No actual bump)	54
6.9	Tire deflection ($z_u - z_r$) of follower vehicle due to spurious preview information (No actual bump)	55
6.10	Preview information by the lead vehicle lagging by 0.005 seconds	55
6.11	Ride quality (\dot{z}_s) of follower vehicle due to small lag in preview information (lag time 0.005s)	56
6.12	Unprung mass deflection (z_u) of follower vehicle due to small lag in preview information (lag time 0.005s)	56
6.13	Suspension deflection ($z_s - z_u$) of follower vehicle due to small lag in preview information (lag time 0.005s)	57
6.14	Tire deflection ($z_u - z_r$) of follower vehicle due to small lag in preview information (lag time 0.005s)	57
6.15	Preview information by the lead vehicle lagging by 0.025 seconds	59
6.16	Ride quality (\dot{z}_s) of follower vehicle due to large lag in preview information (lag time 0.025s)	59
6.17	Unprung mass deflection (z_u) of follower vehicle due to large lag in preview information (lag time 0.025s)	60
6.18	Suspension deflection ($z_s - z_u$) of follower vehicle due to large lag in preview information (lag time 0.025s)	60
6.19	Tire deflection ($z_u - z_r$) of follower vehicle due to large lag in preview information (lag time 0.025s)	61

6.20	Preview information by the lead vehicle leading by 0.005 seconds . . .	61
6.21	Ride quality (\dot{z}_s) of follower vehicle due to small lead in preview information (lead time 0.005s)	62
6.22	Unprung mass deflection (z_u) of follower vehicle due to small lead in preview information (lead time 0.005s)	62
6.23	Suspension deflection ($z_s - z_u$) of follower vehicle due to small lead in preview information (lead time 0.005s)	63
6.24	Tire deflection ($z_u - z_r$) of follower vehicle due to small lead in preview information (lead time 0.005s)	63
6.25	Ride quality (\dot{z}_s) of follower vehicle due to larger lead in preview information (lead time 0.025s)	64
6.26	Unprung mass deflection (z_u) of follower vehicle due to larger lead in preview information (lead time 0.025s)	65
6.27	Suspension deflection ($z_s - z_u$) of follower vehicle due to larger lead in preview information (lead time 0.025s)	65
6.28	Tire deflection ($z_u - z_r$) of follower vehicle due to larger lead in preview information (lead time 0.025s)	66
6.29	Concept of robust preview (*if available)	67
6.30	Estimated road profile by preview-controlled follower vehicle with incorrect preview information for Scenario 1	68
6.31	Estimated road profile by preview-controlled follower vehicle with incorrect preview information for Scenario 2	68
6.32	Ride quality (\dot{z}_s) of follower vehicle when switched from preview-active to active suspension mode	70
6.33	Unprung mass deflection (z_u) of follower vehicle when switched from preview-active to active suspension mode	70

6.34	Suspension deflection ($z_s - z_u$) of follower vehicle when switched from preview-active to active suspension mode	71
6.35	Tire deflection ($z_u - z_r$) of follower vehicle when switched from preview-active to active suspension mode	72
7.1	Rounded pulse	77
7.2	: Schematic Representation of Kalman observer block	78
7.3	Deterministic Road Profile	80
7.4	Estimated states vs. actual states for measurement noise variation (set 2-4). If estimated and actual data is same then the curve should be a 45 degree sharp straight line. Deviation from the line depicts estimation accuracy	82
8.1	Front corner acceleration (\ddot{z}_{f_c}) for Passive and Preview-active suspension system (Preview time 0.28 sec)	93
8.2	Rear corner acceleration (\ddot{z}_{r_c}) for Passive and Preview-active suspension system (Preview time 0.28 sec)	93
8.3	Front tire deflection ($z_{u_{f_c}} - z_{r_{f_c}}$) for Passive and Preview-active suspension system (Preview time 0.28 sec)	94
8.4	Rear tire deflection ($z_{u_{r_c}} - z_{r_{r_c}}$) for Passive and Preview-active suspension system (Preview time 0.28 sec)	94
8.5	Front suspension deflection ($z_{f_c} - z_{u_{f_c}}$) for Passive and Preview-active suspension system (Preview time 0.28 sec)	95
8.6	Rear suspension deflection ($z_{r_c} - z_{u_{r_c}}$) for Passive and Preview-active suspension system (Preview time 0.28 sec)	95
8.7	Pitching acceleration $\ddot{\theta}$ for Passive and Preview-active suspension system (Preview time 0.28 sec)	96

8.8	Front corner acceleration ($\ddot{z}_{f_c}^*$) for Passive and Preview-active suspension system for ride comfort (Preview time 0.28 sec)	97
8.9	Rear corner acceleration ($\ddot{z}_{r_c}^*$) for Passive and Preview-active suspension system for ride comfort (Preview time 0.28 sec)	97
8.10	Front tire deflection ($z_{u_{f_c}} - z_{r_f}$) for Passive and Preview-active suspension system for ride comfort (Preview time 0.28 sec)	98
8.11	Rear tire deflection ($z_{u_{r_c}} - z_{r_r}$) for Passive and Preview-active suspension system for ride comfort (Preview time 0.28 sec)	98
8.12	Pitching acceleration $\ddot{\theta}$ for Passive and Preview-active suspension system for ride comfort (Preview time 0.28 sec)	99
8.13	Front suspension deflection ($z_{u_{f_c}} - z_{r_f}$) for Passive and Preview-active suspension system for ride comfort (Preview time 0.28 sec)	99
8.14	Rear suspension deflection ($z_{u_{r_c}} - z_{r_r}$) for Passive and Preview-active suspension system for ride comfort (Preview time 0.28 sec)	100

Notation

Quarter Car

z_s - Sprung mass displacement (m)

\dot{z}_s - Sprung mass velocity (m/s)

z_u - Unsprung mass displacement (m)

\dot{z}_u - Unsprung mass velocity (m/s)

z_r - Road profile (m)

$(z_s - z_u)$ - Suspension working space (m)

$(z_u - z_r)$ - Dynamic tire deflection (m)

Half Car

z_{fc} - Sprung mass deflection at front corner

\dot{z}_{fc} - Sprung mass velocity at front corner

$z_{u_{fc}}$ - Unsprung mass deflection of front suspension

$\dot{z}_{u_{fc}}$ - Unsprung mass velocity of front suspension

z_{rc} = Sprung mass deflection at rear corner

\dot{z}_{rc} - Sprung mass velocity at rear corner

$z_{u_{rc}}$ - Unsprung mass deflection of rear suspension

$\dot{z}_{u_{rc}}$ - Unsprung mass velocity of rear suspension

Other Symbols

$\xi(t)$ - Process noise

$v(t)$ - Measurement noise

J - LQG cost function

\tilde{L} - Steady-state Kalman observer gain matrix

W - Process noise intensity matrix

V - Measurement noise intensity matrix

Chapter 1

Introduction

The development of suspension systems that can give very good ride comfort along with crisp handling has been the subject of many theoretical and practical investigations for the past three decades. These objectives are hard to implement due to the conflicting nature of the suspension of a vehicle. A brief introduction to the area of vehicle suspension systems is given in the next section followed by a short description of the subject of the current thesis in Section 1.2. Section 1.3 describes the objective of the thesis followed by the contribution of this thesis in Section 1.4 and thesis outline in Section 1.5.

1.1 Vehicle suspension systems

An automotive suspension supports the vehicle body on the axles and contributes to the car's handling, ride comfort for safety and driving pleasure etc. The automotive suspension on a vehicle typically has the following basic tasks [40]

1. Isolate the car body from road disturbances in order to provide good ride quality. Sprung mass acceleration is used to quantify ride quality.

2. Maintain a good road holding. The road holding performance of a vehicle is generally characterized in terms of its cornering, braking and traction abilities, and is quantified by dynamic tire force.
3. Provide good handling and
4. Support the vehicle static weight.

The major problem in designing the suspension of a vehicle is that the designer has to deal with these conflicting demands [1]. Ride comfort and required suspension working space along with dynamic tire forces are important for commercial vehicles. For passenger vehicles, ride comfort and handling are the main concern.

Active or semi-active suspension can be used to improve ride comfort, suspension working space requirement and handling properties instead of using a passive suspension system. An active suspension system has an actuator that can not only dissipate energy but can also supply energy. The actuator can be either hydraulic, pneumatic or electric. A semi-active suspension system can rapidly adjust some of its suspension characteristics, typically the damping factor, as needed in varying road situations. Active suspension shows a superior performance over semi-active and passive suspension system but is generally more expensive compared to passive and semi-active suspension systems.

Design of suitable control strategies for active and semi-active suspensions are a subject of interest for researchers and a lot of effort has been put on this. The majority of control strategies uses 'sky-hook' damping proposed by Karnopp [39]. The performance can be further improved using knowledge of the road surface in front of the actively or semi-actively suspended vehicles and this knowledge is used in the preview control strategy [3, 34]. There are generally two preview concepts. One is using a set of 'look-ahead sensors' at the front bumper of the vehicle to determine the road



Figure 1.1: ‘The military have used convoys for thousands of years to transport troops and equipment during wartime. Convoys are usually groups of vehicles traveling together for increased protection and mutual support’[The Brigade photo, 2011/Patty].

surface, i.e., the preview information [4]. The preview control using this concept is available for both the front and the rear suspension. The second concept is to assume that the road surface at the rear wheels is a delayed version of the front wheels. The preview is available for the rear wheels [5]. Both these concepts have drawbacks. For example, the look-ahead sensor might recognize a heap of leaves as a serious obstacle, while a pot-hole filled with water might not be detected at all [34].

1.2 Convoy vehicle preview control

A new concept of preview is introduced in [12] for a convoy of vehicles where the preview information is generated by the lead vehicle based on its suspension response. The concept is very useful in military convoy vehicles (Figure 1.1) or in an intelligent vehicle highway system (IVHS) to improve safety and avoid vibration-related driver fatigue, injury and crashing.

The idea is to generate the preview information for the follower vehicles based on the

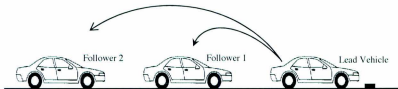


Figure 1.2: Preview control of convoy vehicles with lead follower communication as in [12]

suspension response of the lead vehicle as shown in Figure 1.2 [12]. The lead vehicle has active suspension and the followers use preview-active suspension.

The drawbacks of the system proposed in [12] are,

1. if the generated preview information by the lead vehicle is erroneous then this error will propagate throughout the convoy vehicle system and consequently the performance of the suspension system will be poor;
2. the lead vehicle estimates the road profile but uses the derivative of the road profile which is impractical because the lead vehicle must have some sort of sensor to determine the road for its own use. Moreover, derivative of a noisy signal may generate unusually high signal to noise ratio which may practically lead to instability of the model.

1.3 Research objectives

The main objective of this research is to investigate and design an observer suitable for practical use in a convoy vehicle preview system. The observer must be able to estimate the states along with the unknown input (road profile) for use as preview information and must also be implementable practically. For that purpose, an observer must be designed to reconstruct the road profile irrespective of the suspension system

(active, passive or preview-active) employed on the vehicle. The secondary objectives are to improve the simulation efficiency of preview-active control by decreasing the simulation time requirement. This has been done by implementing a shift register approach with the use of exponential functions as will be described. The research also focuses on the development of control algorithms to design a robust observer for the convoy vehicle preview system so that the effect of the spurious information may be reduced to achieve good performance for the convoy preview-active suspension system.

All results in this thesis are obtained from computer simulations as it was not possible to do the experiments but this will be done in future works.

1.4 Contribution

The contributions of this thesis can be listed as follows

1. A new observer design for a vehicle is proposed and developed that requires no integration or differentiation of the measurements.
2. A discrete preview control algorithm is developed by the use of shift register approach for the continuous time preview function in [2]. This approach increases the simulation efficiency by decreasing the simulation time requirements.
3. A method for robust control for the preview control of convoy vehicles is suggested.
4. Discrete optimal control algorithm is developed for both quarter car and half car models.
5. Effect of variation in measurement noise on the performance of the observer is studied.

6. Simulation is carried out using MATLAB/SIMULINK for the developed observer and control algorithm and the results have been published.

1.5 Thesis outline

This thesis paper is organized as follows. The next chapter provides a brief literature review of preview-active and active suspension research. Chapter 3 describes the vehicle models and their corresponding state space representation used in the simulation. Chapter 4 develops the continuous and discrete optimal control law for a quarter car model and shows the discrete preview-active simulation results. Chapter 5 designs the proposed observer along with a brief background of designing an observer. Chapter 6 shows the general problems associated with convoy vehicle preview and a possible remedy to overcome poor performances by using a switching approach. Chapter 7 studies the effect of variation of measurement noise on the performance of the observer followed by the discrete optimal preview control law for a half car model in Chapter 8. Conclusion and future works are discussed in Chapter 9.

Chapter 2

Literature Review

2.1 Background

Performance of a vehicle suspension system is generally assessed in terms of the competing objectives of sprung mass acceleration (ride quality), suspension deflection (rattle space), and tire deflection (roadholding)[1]. Active suspension systems can manage these tradeoffs better than a passive suspension system, and even further improvements can be attained by the use of preview of the road input [2, 3, 4, 5]. [2] used a quarter car model and showed improvements both in ride quality and road holding performance upon using the preview. Preview-active systems suffer from the practical difficulties involved in measuring the road surfaces by a body-mounted road sensor, since the control law needs information on the road input some distance ahead of the vehicle. Look-ahead sensors on the front bumper, e.g., ultrasonic or laser-based distance sensors, suffer from several limitations like vulnerability to damage and spurious bump detection. For example, a heap of leaves could be shown as a serious obstacle whereas a pothole filled with water may not be detected at all [6, 7]. Furthermore these sensors may not be cost-effective, and mounting them at a fixed distance ahead

of the wheel means that the optimal preview time [8, 9] can only be achieved at a single vehicle speed. Wheelbase preview control has also been studied [10, 7, 11] where rear wheel road input is considered to be the same as the front wheel road input and assumed to be a delayed version of that of the front. Rear suspension performance can be improved through wheelbase preview even if no look-ahead sensors are used; however, front suspension performance is not improved and preview time limitations persist. A convoy, or platoon, of vehicles provides a unique opportunity for preview control of the individual vehicle suspensions. The vehicles travel in close proximity on a similar path, meaning that each should see the same road profile. A scheme is proposed in [12] where the lead vehicle's dynamic responses are used to estimate the road input, which is sent to the follower vehicles in a convoy as the preview information for their suspension controllers. The approach in [12] eliminates the use of look-ahead sensors for vehicles following each other closely. In the military, convoys are used to carry soldiers, weapons and supplies. Many military drivers are young and inexperienced, and driver error has caused many fatal accidents in both peacetime and wartime. Also, the development of an Intelligent Vehicle Highway System (IVHS) with autonomous vehicle platoon remains an active research area. Improving ride quality of closely-spaced vehicles will reduce vibration-related driver fatigue and injury, and improving roadholding and handling during evasive maneuvers will prevent accidents. This thesis reviews the system originally proposed in [12] and presents a new and improved estimator to reconstruct road profiles with a wide range of discrete bumps. The estimator works for vehicles with passive, active, or preview-active suspensions. Any vehicle in the platoon, not just the leader, can estimate the road profile for use by vehicles behind. A given vehicle can then use preview information from the convoy leader, the vehicle immediately preceding it, or any combination of preceding vehicles. Multiple sources of preview information allow variation in effective

preview time, while also increasing robustness to sensor malfunction on an individual vehicle, or to changes in terrain due to obstacles being dislodged mid-convoy. If a vehicle compares its own terrain estimate to that from the preview information, and detects discrepancy, then its suspension control can revert to conventional active and that vehicle can initiate new preview information for its followers.

2.2 Literature review

Bender [3], followed by many others, such as [2, 5, 7], showed significant improvements in ride quality (as indicated by body acceleration) when using preview of the upcoming terrain in the suspension controller design. Hac [2] reported reduction in tire deflection, and suggested that a primary benefit of preview suspension could be in reducing dynamic tire deflection as the suspension “anticipates” upcoming discrete road events. References[2, 5] report the presence of an optimal preview time. [5] suggested that performance improvements can be done for high frequency road inputs even with shorter preview time. [5] considered both quarter car and half car model and showed that improvements can be achieved with a step type road input. More recent works on preview control such as [13, 14, 15, 16, 9, 17] report performance improvements in the three competing suspension control objectives mentioned in the introduction. [13] implemented a composite-sensor system to sense the road for preview and suggested preview control algorithm for a full car model. [14] considered the sensors to be mounted in the front bumper and use the delayed version of the sensed road in rear wheels and suggested improvements along with reduction in energy consumption. [15] simulated output feedback H_∞ preview control where constrain on suspension working space is associated in the control algorithm. Actuator dynamics provide a practical limitation on preview suspension performance. El Madany et al.

[18] and Pilbeam and Sharp [8] studied slow active suspension systems with preview, with [18] showing that good performance can be achieved using low-bandwidth actuation. Pilbeam [8] also observed an optimal preview time and showed that lower bandwidth requires more preview time but uses less energy than that of higher bandwidth systems. References [6, 19, 20, 21] showed that the use of preview can effectively overcome actuator delay, thereby improving performance. [21] implemented preview control on an experimental vehicle with sensor mounted on front bumper and showed that vertical acceleration of the experimental preview controlled vehicle is decreased by 25% than a non-preview controlled one on a downgrade road. Al Akbari et al. [15] also compared different preview control methods. Vahidi and Eskandarian [22] studied the effect of uncertainties in preview-active suspension system, showing limits on preview uncertainty beyond which the benefits of preview are negated. Types of uncertainties studied by [22] are preview sensor noise and presence of false objects on the road. The issue of preview information timing was not considered. This thesis does a small parametric study of the effect of timing errors, as such errors are unique to the proposed convoy implementation where look-ahead sensors are not mounted to each vehicle.

Power consumption is an important consideration when considering practical feasibility of preview suspensions. Hac [2] and Marzbanrad et al. [14] showed lower power consumption for preview-active suspensions compared to conventional active suspensions.

Despite the theoretical benefits of preview, practical implementation has been limited. Hardware implementations of preview are shown in [20, 23, 24], with [20] describing wheelbase preview in a half car rig with hardware-in-the-loop simulation. Improvements in rms body acceleration at the drive axle were 15.4%, 18.2% and 16.2% for motorway, principal and minor roads respectively. Akbari et al. [24] implemented

multi objective H_∞/GH_2 preview control on an experimental quarter-car setup and showed an improvement of 22% in ride comfort. Langlois et al. [23] implemented preview controlled active suspension in an off-road vehicle with ultrasonic look-ahead sensors in front of the vehicle. Results from [23] showed 15% improvement in ride quality over passive suspension and 4% over active suspension without preview. The small improvement over active suspension was likely due to a simplified controller that could be implemented without significant modifications to their existing hardware. Preview has not infiltrated the automotive industry as much as conventional active or semi-active suspension, despite the industry's potential use of custom-designed hardware, due to aforementioned challenges such as sensor cost, durability, and accuracy. It is desirable to replace look-ahead sensors with road estimators as in [12, 7] to generate the preview information.

A number of methods can be found in the literature to estimate an unknown input [25, 26, 27, 28]. However, these require the differentiation of measurements, which poses serious challenges to maintaining an acceptable signal to noise ratio. Integrating measurements such as accelerations requires elimination of drift. In [12], a continuous time Kalman-Bucy observer is designed where a virtual lead car with active suspension generates the road profile and estimates the vehicle states based on its dynamic motion and feeds it to a preview-controlled follower car. The implementation in [12] required differentiating the road estimate, and the continuous-time Matlab simulation was prohibitively slow. To summarize, prior research motivates the use of preview suspension if practical implementation issues could be resolved. A road estimator that requires only practically-available measurements, and no differentiation or integration thereof, is developed and applied to a simulated convoy scenario in this thesis. The estimator replaces the look-ahead sensor. To improve the computational efficiency of the continuous time preview function from [2], as implemented in [12], a discrete time

model with a shift register algorithm for preview function generation is formulated. Such preview, without look-ahead sensors and with robustness to mid-convoy terrain changes, would have potential safety benefits to the military and to automated highway systems. Eventual improvements in vehicle-to-vehicle communication, active cruise control, and global positioning systems could allow discrete road events estimated through vehicle dynamic response to be useful as preview information for following vehicles even if they were not part of a formal convoy or fully automated highway. Preview control of active suspension for convoys not only improves the performance of individual vehicle but can also increase the fuel efficiency of the convoy system. Al Alam et al. [29] showed that use of preview information for adaptive cruise control system can reduce fuel consumption by 3.8%-7.7% depending on the vehicle weight.

[41] developed a neural network based algorithm for preview semi-active suspension based on halfcar model. In [41] wheelbase preview control for a semi-active halfcar model is simulated. Simulated results from neural network control is compared to an adaptive PID preview control algorithm.

2.3 Organization of the report

Chapter 3 will now describe the vehicle model and states, and implement the plant and preview controller in discrete time using a shift register approach to achieve significant increases in computational efficiency.

In this thesis both quarter car and half car representation of a vehicle is used as the model for simulating the convoy-vehicle preview scenario. The quarter car reduces the dimension of the optimal control problem compared to a half or full car. Quarter car-based optimal suspension controllers can effectively control pitch and roll in half-

cars [23, 30]. Half car model is simulated for preview with half car control algorithm and results will be discussed in a later chapter.

Chapter 3

Vehicle Models and State Space Representation

Study of the active suspension requires vehicle models in order to illustrate the dynamics of the suspension in different types of road irregularities. Generally three types of vehicle models are used in the study of the suspension. They are

- (i) Quarter car model
- (ii) Half car model
- (iii) Full car model

Quarter car models capture the dynamics of the car in the vertical direction only. So study of the quarter car model is used to improve ride-comfort, road holding and suspension working space of the vehicle. Half car models capture the dynamics in longitudinal and vertical direction (pitch and heave motions). Full car models are used to study pitch, roll and heave motions simultaneously.

3.1 Vehicle models

Only two-dimensional (2-D) models are used in this thesis to study the dynamic behavior in longitudinal and vertical directions (heave and pitch). This is because the benefits of active suspension are supposed to be gained specially in these two directions. In this chapter, dynamic equations of a quarter car vehicle model and half car model are generated and the state space representation of the system is described.

3.1.1 Quarter car model

Figure 3.1 shows a 2-DOF quarter car model with active suspension. It represents the automotive system at each wheel, i.e., the motion of the axle and of the vehicle at any one of the four wheels of the vehicle. The suspension consist of a spring (k_s), a passive damper (b_s) and an active force actuator (u) placed in parallel with the passive damper and the spring. The active force u can be set to zero to imitate a passive suspension. The sprung mass m_s represents the quarter car equivalent of the total body mass of the vehicle. The unsprung mass m_u represents the equivalent mass due to the axle and tire. The vertical stiffness of the tire is represented by the spring k_t . The variables z_s , z_u and z_r represent the vertical displacements from the static equilibrium of the sprung mass, unsprung mass and the road elevation respectively. The equations of motion can be written as

$$m_s \ddot{z}_s + k_s(z_s - z_u) + b_s(\dot{z}_s - \dot{z}_u) - u = 0 \quad (3.1)$$

$$m_u \ddot{z}_u + k_s(z_u - z_s) + k_t(z_u - z_r) + b_s(\dot{z}_s - \dot{z}_u) + u = 0 \quad (3.2)$$

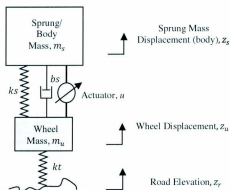


Figure 3.1: 2-DOF quarter car model

3.1.1.1 State space representation of quarter car model

It is beneficial to represent the system given by eqn 3.2 in state space form. Eqn 3.2 can be written in state space form as

$$\dot{x}(t) = Ax(t) + Bu(t) + Fz_r(t) \quad (3.3)$$

where the state vector is $x(t) = \begin{bmatrix} z_s & \dot{z}_s & z_u & \dot{z}_u \end{bmatrix}^T$ and

z_s = Sprung mass deflection

\dot{z}_s = Sprung mass velocity

z_u = Unsprung mass deflection

\dot{z}_u = Unsprung mass velocity

The matrices A , B , and F are given by

$$A = \begin{bmatrix} 0 & 1 & 0 & 0 \\ -\frac{k_s}{m_s} & -\frac{b_s}{m_s} & \frac{k_s}{m_s} & \frac{b_s}{m_s} \\ 1 & 0 & 0 & 0 \\ \frac{k_s}{m_u} & \frac{b_s}{m_u} & -\frac{(k_s+k_t)}{m_u} & -\frac{b_s}{m_u} \end{bmatrix}, \quad B = \begin{bmatrix} 0 \\ \frac{1}{m_s} \\ 0 \\ -\frac{1}{m_s} \end{bmatrix}, \quad F = \begin{bmatrix} 0 \\ 0 \\ 0 \\ \frac{k_t}{m_u} \end{bmatrix}$$

Eqn 3.3 is a continuous time state space representation of the system.

3.1.2 Half car model

Consider the half car model as shown in Figure 3.2. The front suspension consists of a spring (k_{fs}), a passive damper (b_{fs}) and an active force actuator (U_f) placed in parallel with the passive damper and the spring. The rear suspension also consists of a spring (k_{rs}), a passive damper (b_{rs}) and an active force actuator (U_r) placed in parallel with the passive damper and the spring. The active force U_f and U_r can be set to zero to imitate a passive half car suspension. The pitch motion of the vehicle is represented by θ_b . The sprung mass M_s represents the quarter car equivalent of the total body mass of the vehicle. The front unsprung mass m_{uf} and the rear unsprung mass m_{ur} represents the equivalent mass due to the axle and tire at the front and the rear of the vehicle respectively. The vertical stiffness of the front and rear tire is represented by the spring k_{tf} and k_{tr} respectively. The variables Z_b represents the vertical displacement of the vehicle body from the static equilibrium. The variables z_{fc} and z_{rc} represents the vertical displacement of the vehicle body from the static equilibrium for the front and rear corner of the vehicle respectively. The variables z_{ufc} and z_{urc} represents the vertical displacement of the unsprung mass for the front and rear suspension respectively with l_f and l_r are being the distances of front and rear corner from the mass center respectively. For small pitching angles (θ_b)

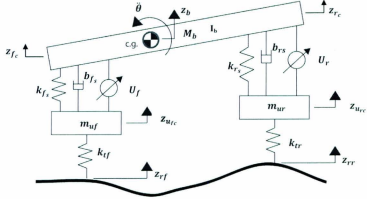


Figure 3.2: Half car model

$$z_{fc} = Z_b - l_f \theta_b \quad (3.4)$$

$$z_{rc} = Z_b + l_r \theta_b \quad (3.5)$$

$$m_{uf} \ddot{z}_{uf} = k_{if}(z_{rf} - z_{uf}) - [U_f + k_{fs}(z_{uf} - z_{fc}) + b_{fs}(\dot{z}_{uf} - \dot{z}_{fc})] \quad (3.6)$$

$$m_{ur} \ddot{z}_{ur} = k_{if}(z_{rc} - z_{ur}) - [U_r + k_{rs}(z_{ur} - z_{rc}) + b_{rs}(\dot{z}_{ur} - \dot{z}_{rc})] \quad (3.7)$$

$$\begin{aligned} \ddot{z}_{fc} = & \left(\frac{1}{M_b} + \frac{l_f^2}{I_b} \right) [U_f + k_{fs}(z_{uf} - z_{fc}) + b_{fs}(\dot{z}_{uf} - \dot{z}_{fc})] + \left(\frac{1}{M_b} \right. \\ & \left. - \frac{l_f l_r}{I_b} \right) [U_r + k_{rs}(z_{ur} - z_{rc}) + b_{rs}(\dot{z}_{ur} - \dot{z}_{rc})] \end{aligned} \quad (3.8)$$

$$\begin{aligned} \ddot{z}_{rc} = & \left(\frac{1}{M_b} - \frac{l_f l_r}{I_b} \right) [U_f + k_{fs}(z_{uf} - z_{fc}) + b_{fs}(\dot{z}_{uf} - \dot{z}_{fc})] + \left(\frac{1}{M_b} \right. \\ & \left. + \frac{l_r^2}{I_b} \right) [U_r + k_{rs}(z_{ur} - z_{rc}) + b_{rs}(\dot{z}_{ur} - \dot{z}_{rc})] \end{aligned} \quad (3.9)$$

here I_b is the pitching moment of inertia and z_{rj} and z_{rr} are the road elevation at front and rear wheel respectively.

3.1.2.1 State space representation of half car model

State space form for half car model can be generated with either eight states (four states for each corner suspension) or ten states (includes pitch angle and the pitch velocity of the car along with the other eight states)¹. A state space model with eight states can be written as

$$\dot{x}(t) = \alpha x(t) + \beta u(t) + \gamma z_r(t) \quad (3.10)$$

where $x(t) = \left[z_{f_c} \quad z'_{f_c} \quad z_{u_{f_c}} \quad z'_{u_{f_c}} \quad z_{r_c} \quad z'_{r_c} \quad z_{u_{r_c}} \quad z'_{u_{r_c}} \right]^T$ and

z_{f_c} = Sprung mass deflection at front corner

z'_{f_c} = Sprung mass velocity at front corner

$z_{u_{f_c}}$ = Unsprung mass deflection of front suspension

$z'_{u_{f_c}}$ = Unsprung mass velocity of front suspension

z_{r_c} = Sprung mass deflection at rear corner

z'_{r_c} = Sprung mass velocity at rear corner

$z_{u_{r_c}}$ = Unsprung mass deflection of rear suspension

$z'_{u_{r_c}}$ = Unsprung mass velocity of rear suspension

$$u(t) = \begin{bmatrix} U_f & U_r \end{bmatrix}^T$$

$$z_r(t) = \begin{bmatrix} z_{r_f} & z_{r_r} \end{bmatrix}^T$$

The matrices α , β and γ are given by

¹Please note that number of states can be varied

$$\alpha = \begin{bmatrix} 0 & 1 & 0 & 0 & 0 & 0 & 0 & 0 \\ -\pi_1 k_{fs} & -\pi_1 b_{fs} & \pi_1 k_{fs} & \pi_1 b_{fs} & -\pi_2 k_{rs} & -\pi_2 b_{rs} & \pi_2 k_{rs} & \pi_2 b_{rs} \\ 0 & 0 & 0 & 1 & 0 & 0 & 0 & 0 \\ \frac{k_{fs}}{m_{sf_c}} & \frac{b_{fs}}{m_{sf_c}} & -\frac{(k_{fs}+k_{ff})}{m_{sf_c}} & \frac{-b_{fs}}{m_{sf_c}} & 0 & 0 & 0 & 0 \\ 0 & 0 & 0 & 0 & 0 & 1 & 0 & 0 \\ -\pi_2 k_{fs} & -\pi_2 b_{fs} & -\pi_2 b_{fs} & \pi_2 b_{fs} & -\pi_3 k_{rs} & -\pi_3 b_{rs} & \pi_3 k_{rs} & \pi_3 b_{rs} \\ 0 & 0 & 0 & 0 & 0 & 0 & 0 & 1 \\ 0 & 0 & 0 & 0 & \frac{k_{rs}}{m_{sr_c}} & \frac{b_{rs}}{m_{sr_c}} & -\frac{(k_{rs}+k_{rr})}{m_{sr_c}} & \frac{k_{rs}}{m_{sr_c}} \end{bmatrix},$$

$$\beta = \begin{bmatrix} 0 & 0 \\ \pi_1 & \pi_2 \\ 0 & 0 \\ -\frac{1}{m_{sf_c}} & 0 \\ 0 & 0 \\ \pi_2 & \pi_3 \\ 0 & 0 \\ 0 & -\frac{1}{m_{sr_c}} \end{bmatrix}, \quad \gamma = \begin{bmatrix} 0 & 0 \\ 0 & 0 \\ 0 & 0 \\ \frac{k_{ff}}{m_{sf_c}} & 0 \\ 0 & 0 \\ 0 & 0 \\ 0 & 0 \\ 0 & \frac{k_{rr}}{m_{sr_c}} \end{bmatrix}$$

π_1 , π_2 and π_3 are given by

$$\pi_1 = \frac{1}{M_b} + \frac{l_f^2}{I_b}, \pi_2 = \frac{1}{M_b} - \frac{l_f l_r}{I_b}, \pi_3 = \frac{1}{M_b} + \frac{l_r^2}{I_b}$$

Eqn 3.10 is a continuous time state space representation of a half car model with the state space matrices α, β and γ as shown above.

3.2 Vehicle parameters

Vehicle parameters for simulating the quarter car suspension model are taken from [2]. The table below shows the parameters used

Table 3.1: Quarter car model parameters

Symbol	Description	Value
m_s	Sprung mass	250 kg
m_u	Unsprung mass	45 kg
k_s	Suspension stiffness	16000 N/m
k_t	Tire stiffness	160000 N/m
b_s	Damping coefficient	1000 N/m

Vehicle parameters for the half car model is based on a light truck model taken from [41]. Parameters are listed in table 3.2.

Table 3.2: Half car model parameters

Symbol	Description	Value
l_f	Distance from front axle to mass center	1444.4 mm
l_r	Distance from front axle to mass center	1305.6 mm
M_s	Vehicle body mass	803.7 kg
$m_{w_{fc}}$	Front wheel mass	90 kg
$m_{w_{rc}}$	Rear wheel mass	115 kg
I_b	Pitching moment of inertia	3128.1 kg
k_{fs}	Front suspension stiffness	130 kN/m
k_{rs}	Rear suspension stiffness	85 kN/m
b_{fs}	Front damping coefficient	3040 Ns/m
b_{rs}	Rear damping coefficient	3040 Ns/m
k_{tf}	Front Tire stiffness	405 kN/m
k_{tr}	Rear Tire stiffness	405 kN/m

Chapter 4

Optimal Preview Control of Convoy Vehicle Suspension: Quarter Car Model

The objective of this chapter is to establish an optimal preview control law for a convoy vehicle system as given in [2] using quarter car models. A virtual convoy system with a lead vehicle and corresponding follower vehicle is shown in Figure 4.1. The road profile for the follower vehicle is generated by the lead vehicle based on its suspension response. In this chapter we will consider that the road profile is estimated by the lead vehicle and fed to the follower vehicle, and develop the control law for the optimal preview control of the follower vehicle. The basis of optimal preview control is based on LQR (Linear Quadratic Regulator) theory which is well established control theory found in the literature.

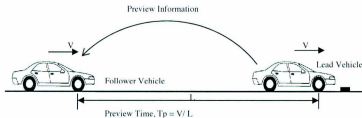


Figure 4.1: Lead-follower arrangement for convoy preview

4.1 Development of optimal control law

Consider the quarter car model shown in Figure 3.1. Equations of motion are given by 3.1 and 3.2. The state space form is also shown in the previous chapter. The optimal control problem is to optimize the suspension system with respect to road holding, ride comfort and suspension working space. In addition, the magnitude of the control force must be constrained to the limits of the actuator. A performance index can be defined based on the above parameters [2],

$$J = \lim_{T \rightarrow \infty} \frac{1}{2T} \int_0^T E[\dot{z}_s^2 + \mu_1 \{z_s(t) - z_u(t)\}^2 + \mu_2 \{z_u(t) - z_r(t)\}^2 + \mu_3 u(t)^2] dt \quad (4.1)$$

where E is the expectation, and constants μ_x are the weighting parameters selected by the designer. (4.1) can be represented in matrix form upon substitution of (3.1) and (3.2),

$$J = \lim_{T \rightarrow \infty} \frac{1}{2T} \int_0^T E[x^T Q_1 x + u^T R u + 2x^T N u + 2x^T Q_{12} z_r + z_r^T Q_2 z_r] dt \quad (4.2)$$

where

$$Q_1 = \begin{bmatrix} \frac{k_z^2}{m_z^2} + \mu_1 & \frac{b_z k_x}{m_z^2} & -\frac{k_z^2}{m_z^2} - \mu_1 & -\frac{b_z k_x}{m_z^2} \\ \frac{b_z k_x}{m_z^2} & \frac{b_z^2}{m_z^2} & -\frac{b_z k_x}{m_z^2} & -\frac{b_z^2}{m_z^2} \\ -\frac{k_z^2}{m_z^2} - \mu_1 & -\frac{b_z k_x}{m_z^2} & \mu_1 + \mu_2 + \frac{k_z^2}{m_z^2} & \frac{b_z k_x}{m_z^2} \\ -\frac{b_z k_x}{m_z^2} & -\frac{b_z^2}{m_z^2} & \frac{b_z k_x}{m_z^2} & \frac{b_z^2}{m_z^2} \end{bmatrix}$$

$$R = \frac{1}{m_z^2} + \mu_3, \quad N = \begin{bmatrix} -\frac{k_z^2}{m_z^2} \\ -\frac{b_z}{m_z^2} \\ \frac{k_z^2}{m_z^2} \\ \frac{b_z}{m_z^2} \end{bmatrix}$$

and

$$Q_{12} = \begin{bmatrix} 0 & 0 & -\mu_2 & 0 \end{bmatrix}^T, \quad Q_2 = \mu_2$$

The last term of the performance index can be neglected because of the fact that the control input does not affect the road irregularities. The objective of linear optimal preview control is to find a control force, u so that the performance equation is minimized for an entire class of stochastic inputs $z_r(t)$. The control force $u(t)$ must contain a feedback term which takes the current states using optimal LQR theory [42] and a feed-forward term from the knowledge of the road ahead.

For the linear time invariant system given by (3.3) the measurement equation can be written as

$$y = Cx + Du + v \quad (4.3)$$

where v is the measurement noise from the sensors. Here the measured quantities are the states $x(t)$. Suppose the road profile is available up to time τ_p into the future, i.e.,

$z_r(\tau)$ is available where $\tau \in [t, t + \tau_p]$, and all the states at time t are present. Then the solution of the linear deterministic optimal preview control is given as [2]

$$u_o(t) = -R^{-1}[(N^T + B^T \bar{P})x(t) + B^T r(t)] \quad (4.4)$$

where \bar{P} is the solution of the algebraic Riccati equation [42] given by

$$\bar{P}A_n + A_n^T \bar{P} + \bar{P}BR^{-1}B^T \bar{P} + Q_n = 0 \quad (4.5)$$

and the preview function is

$$r(t) = \int_0^{\tau_p} e^{A_n^T \sigma} (\bar{P}F + Q_{12})z_r(t + \sigma) d\sigma \quad (4.6)$$

where

$$A_n = A - BR^{-1}N^T \text{ and } Q_n = Q_1 - NR^{-1}N^T$$

The feedback part of (4.4) is

$$u_{ffo}(t) = -R^{-1}(N^T + B^T \bar{P})x(t) \quad (4.7)$$

The feedback gains can be found from the solution of the LQR problem [42, 33] that minimizes the performance index J . These gains are multiplied to the states as shown in eqn 4.7. The feed-forward term is

$$u_{ffo}(t) = -R^{-1}B^T r(t) \quad (4.8)$$

The vector $r(t) \in \mathfrak{R}^n$ uses all the available future information about the road input z_r .

4.7 and 4.8 are the continuous time optimal preview control law for the follower vehicle in a convoy vehicle system. At each step the preview control law requires the integration of the preview function given by 4.6 over the designed preview time. This requires higher simulation time. To improve simulation time the continuous preview function has been discretized by the use of exponential functions (see Appendix), and a variable shift register algorithm implemented, with discretization done using MATLAB.

4.2 Discretization of continuous system

Consider again the continuous system (3.3)

$$\dot{x}(t) = Ax(t) + Bu(t) + Fz_r(t)$$

with measurements

$$y = Cx(t) + Du(t) + v(t)$$

where $v(t)$ is a white noise process with variance Q . We will consider the road profile to be an input to the system which is unknown at this point and will be estimated. The estimators will be optimal for random inputs, but we will also consider deterministic road inputs such as traffic humps, potholes, etc. The continuous system time response is given by [31, 32],

$$x(t) = e^{A(t-t_0)}x(t_0) + \int_{t_0}^t e^{A(t-\tau)}Bu(\tau) d\tau + \int_{t_0}^t e^{A(t-\tau)}Fz_r(\tau) d\tau \quad (4.9)$$

Let $t_0 = kT$, $t = (k+1)T$ for an integer k . Defining the sampled state function as $x_k \triangleq x(kT)$ we can write

$$x_{k+1} = e^{AT} x_k + \int_{kT}^{(k+1)T} e^{A[(k+1)t-\tau]} B u(\tau) d\tau + \int_{kT}^{(k+1)T} e^{A[(k+1)t-\tau]} F z_r(\tau) d\tau \quad (4.10)$$

Assuming that the control input $u(t)$ is reconstructed from the discrete control sequence u_k by using a zero order hold, and also that the unknown road input $z_r(t)$ is reconstructed from a discrete measurement sequence $z_{r,k}$ using a zero order hold, $u(\tau)$ and $z_r(\tau)$ have constant values of $u(kT) = u_k$ and $z_r(kT) = z_{r,k}$ respectively over the integration interval. The discrete time equation becomes

$$x_{k+1} = e^{AT} x_k + \int_{kT}^{(k+1)T} e^{A[(k+1)t-\tau]} B d\tau \cdot u_k + \int_{kT}^{(k+1)T} e^{A[(k+1)t-\tau]} F d\tau \cdot z_{r,k} \quad (4.11)$$

On changing the variables twice ($\lambda = \tau - kT$ and then $\tau = T - \lambda$) the above equation can be written as

$$x_{k+1} = e^{AT} x_k + \int_0^T e^{A\tau} B d\tau \cdot u_k + \int_0^T e^{A\tau} F d\tau \cdot z_{r,k} \quad (4.12)$$

The equivalent discrete form of the system is then

$$x_{k+1} = \Phi x_k + \Gamma u_k + \Psi z_{r,k} \quad (4.13)$$

where

$$\begin{aligned}\Phi &= e^{AT} = I + AT + \frac{A^2T^2}{2!} + \dots \\ \Gamma &= \int_0^T e^{A\tau} B d\tau = BT + \frac{ABT^2}{2!} + \dots \\ \Psi &= \int_0^T e^{A\tau} F d\tau = FT + \frac{AFT^2}{2!} + \dots\end{aligned}$$

Discretization of the measurement equation is straightforward since it has no dynamics:

$$z_k = Cx_k + Du_k + v_k \quad (4.14)$$

The covariance \mathcal{R} of v_k in terms of the given covariance \mathcal{Q} can be found easily from

$$\mathcal{R} = \frac{\mathcal{Q}}{T}$$

For the current analysis the steady state LQR gains from the continuous system are used for the feedback part of the actuator force given by (4.7). The feed-forward part given by (4.8) contains the preview function

$$r(t) = \int_0^{T_p} e^{A_r \tau} (\bar{P}F + Q_{12}) z_r(t + \sigma) d\sigma$$

This must also be discretized. The discrete preview function at any step can be found from the preview function value calculated at the previous step and is given by (see Appendix)

$$r_{k+1} = \mathcal{F}^{-1} r_k - \mathcal{F}^{-1} z_{r_k} \mathcal{M} \Delta t + \mathcal{F}^n z_{r_{k+n+1}} \mathcal{M} \Delta t \quad (4.15)$$

where

$$\mathcal{F} = e^{A_c T \Delta t}$$

$$\mathcal{M} = \bar{P}F + Q_{12}, \quad T_p = n\Delta t$$

Here Δt can be the same as the discretization time step T . A more general form of the preview function calculation (variable shift register approach) can be written as (see Appendix)

$$r_{k+p} = \mathcal{F}^{-(p+q)} r_{k-q} - S_1 + S_2 \quad (4.16)$$

where the preview information at r_{k+p} is to be determined given that the preview information at r_{k-q} is known and

$$S_1 = \sum_{i=p+q, j=0}^{1, p+q-1} \mathcal{F}^{-i} z_{r_{k-q+j}} \mathcal{M} \Delta t$$

$$S_2 = \sum_{i=p+q, j=0}^{1, p+q-1} \mathcal{F}^{n-i+1} z_{r_{k+n+j}} \mathcal{M} \Delta t$$

where $p + q < n$.

4.3 Simulation results

Simulation is carried out using MATLAB for the convoy vehicle scenario where the follower vehicle receives the preview information, i.e., the road profile, from the lead vehicle. Vehicle parameters are listed in table 3.1 on page 21. The road input con-

sidered here is a single half-sinusoidal bump expressed using the following equation [2],

$$z_r(t) = \begin{cases} c[1 - \cos 40\pi(t - 3)], & t \in [3, 3.05] \\ 0, & \text{otherwise} \end{cases}$$

where $2c$ is the height of the bump in meters and t is the time in seconds. A bump height of 10 cm has been considered for simulation with vehicle velocity 20 m/s .

4.3.1 Road holding weighting factors

Simulation results are shown in this section for the optimal quarter car gains found using weighting factors which puts more emphasis on road tracking, i.e., road holding than ride comfort. For active and preview active suspension the weights of the performance index are $\mu_1 = 10^3$, $\mu_2 = 10^5$ and $\mu_3 = 0$. Figure 4.2 shows the vertical position of the wheel z_u (unsprung mass displacement) along with the road elevation z_r . Figure 4.3 shows the vertical acceleration of the vehicle body \ddot{z}_s for passive, active and preview active suspension. The force actuator has been saturated by clipping the force at $\pm 4000N$, i.e., $u \in [-4000N, 4000N]$. A preview time of 0.2 seconds has been used. Figure 4.4 shows tire deflection, $(z_u - z_r)$ along with the road elevation, z_r and Figure 4.5 shows suspension deflection, $(z_s - z_u)$ along with the road elevation z_r .

From the results it is evident that preview-active control is better compared to conventional active and passive suspension systems. Figure 4.4 shows better road tracking, with improvements of 46.47% and 23.37% in positive and negative peak magnitudes respectively compared to a passive system and 42.47% and 23.78% compared to an active system. Comparison of suspension deflection (Figure 4.5) shows 51.12% and

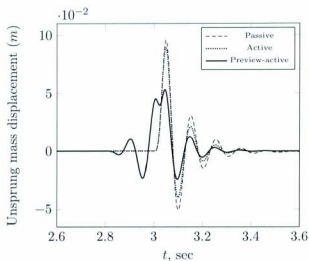


Figure 4.2: Wheel displacement (z_u) for Passive, Active and Preview-active suspension system (Preview time 0.2 sec)

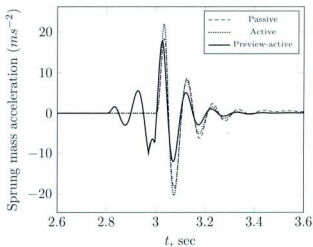


Figure 4.3: Sprung mass acceleration (\ddot{z}_s) for Passive, Active and Preview-active suspension system (Preview time 0.2 sec)

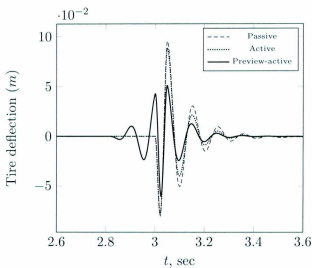


Figure 4.4: Tire deflection ($z_u - z_r$) for Passive, Active and Preview-active suspension system (Preview time 0.2 sec)

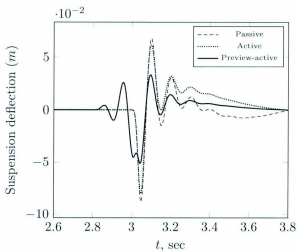


Figure 4.5: Suspension deflection ($z_s - z_u$) for Passive, Active and Preview-active suspension system (Preview time 0.2 sec)

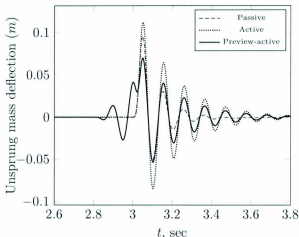


Figure 4.6: Wheel displacement (z_w) for Passive, Active and Preview-active suspension system for ride comfort(Preview time 0.2 sec)

41.89% improvement over passive and 46.36% and 36.32% over the active system. Relatively less but still significant improvement in ride comfort have been observed from Figure 4.3, which is justified given that the chosen gain parameters emphasize road holding.

4.3.2 Ride quality weighting factors

Weighting factors that put more emphasis on ride comfort have also been considered for simulation: $\mu_1 = 0.5$, $\mu_2 = 10^4$ and $\mu_3 = 0.000001$. Results are shown in Figure 4.6-4.9.

Figure 4.7 shows the comparison of ride comfort for all three systems. An improvement of 57.03% in positive and 62.92% in negative peak magnitudes compared to a passive suspension system has been observed for preview-active suspension, which is 13.91% and 38.93% more than for an active suspension system. Reasonable improvements are observed for road holding and suspension deflection as well (Figures 4.8-4.9). While

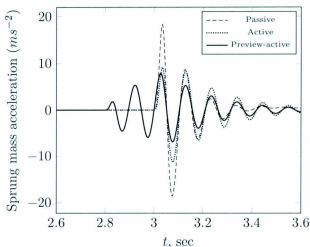


Figure 4.7: Sprung mass acceleration (\ddot{z}_s) for Passive, Active and Preview-active suspension system for ride comfort(Preview time 0.2 sec)

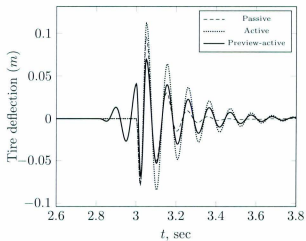


Figure 4.8: Tire deflection ($z_u - z_r$) for Passive, Active and Preview-active suspension system for ride comfort(Preview time 0.2 sec)

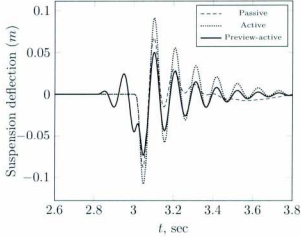


Figure 4.9: Suspension deflection ($z_s - z_u$) for Passive, Active and Preview-active suspension system for ride comfort(Preview time 0.2 sec)

the active suspension system performs worse than the passive suspension system for roadholding and suspension deflection for the ride quality-focused set of performance indices, the preview-active system shows improvement in all areas.

4.4 Effect of preview time

The effect of preview time is investigated by quantifying the improvement in peak magnitudes of sprung mass acceleration, suspension deflection, and tire deflection for three preview times: 0.1, 0.2 and 0.3 seconds. Improvement for any particular state x_i compared to passive and active has been calculated using the following relationship

$$I_p = \frac{\max(x_{i,passive/active}) - \max(x_{i,preview})}{\max(x_{i,passive/active})} \times 100\% \quad (4.17)$$

$$I_n = \frac{\min(x_{i,passive/active}) - \min(x_{i,preview})}{\min(x_{i,passive/active})} \times 100\% \quad (4.18)$$

where I_p and I_n are the performance improvements in the positive and the negative peak respectively.

Table 4.1: Improvements in performance compared to passive system for road holding weighting factors

Preview time	Description	Improvements(I_p, I_n)%
0.1s	Suspension deflection	(46.17, 41.64)
	Road holding	(43.75, 21.85)
	Ride quality	(-2.30, 32.39)
0.2s	Suspension deflection	(51.12, 41.89)
	Road holding	(46.47, 23.37)
	Ride quality	(3.48, 35.45)
0.3s	Suspension deflection	(51.12, 41.99)
	Road holding	(46.59, 23.45)
	Ride quality	(3.91, 35.52)

Table 4.2: Improvements in performance compared to active system for road holding weighting factors

Preview time	Description	Improvements(I_p, I_n)%
0.1s	Suspension deflection	(40.93, 36.05)
	Road holding	(39.55, 22.27)
	Ride quality	(14.69, 38.48)
0.2s	Suspension deflection	(46.36, 36.32)
	Road holding	(42.47, 23.78)
	Ride quality	(19.51, 41.27)
0.3s	Suspension deflection	(46.36, 36.43)
	Road holding	(42.60, 23.86)
	Ride quality	(19.87, 41.33)

The vehicle velocity considered for simulation is 20 m/s. A preview time of 0.3 seconds gives the best overall performance; however, the point of the tables is that the ability to vary preview time is advantageous. The method of this paper allows preview information from different possible lead vehicles to be used, allowing preview time to be varied in an actual implementation. Different forward speeds will have

Table 4.3: Improvements in performance compared to passive system for ride quality weighting factors

Preview time	Description	Improvements(I_p, I_n)%
0.1s	Suspension deflection	(9.17, 6.91)
	Road holding	(15.16, 9.75)
	Ride quality	(48.99, 56.92)
0.2s	Suspension deflection	(25.83, 16.22)
	Road holding	(26.96, 12.50)
	Ride quality	(57.03, 62.92)
0.3s	Suspension deflection	(32.47, 18.56)
	Road holding	(31.12, 13.04)
	Ride quality	(59.99, 64.92)

different optimal preview times, again motivating the departure from fixed look-ahead sensors for which a single preview time is associated with a given vehicle velocity. It has also been found in our simulations that there exists a trend in the performance improvement such that if the vehicle speed is increased over a limited range for the same single bump, then preview suspension performance increases.

Table 4.4: Improvements in performance compared to passive system for ride quality weighting factors

Preview time	Description	Improvements(I_p, I_n)%
0.1s	Suspension deflection	(32.71, 24.14)
	Road holding	(27.70, 15.91)
	Ride quality	(-2.21, 29.04)
0.2s	Suspension deflection	(45.05, 31.73)
	Road holding	(37.76, 18.47)
	Ride quality	(13.91, 38.93)
0.3s	Suspension deflection	(49.97, 33.64)
	Road holding	(41.30, 18.99)
	Ride quality	(19.83, 42.23)

Chapter 5

Observer Design

The preceding chapter showed significant improvements from using a preview-active suspension system. Noise-free sensors and perfectly measured preview information were assumed. However, in practice it is not possible to measure all the states. Sensors are not noise-free, and sensor data may require integration or differentiation to get the system states. Integration introduces drift and differentiation amplifies the error and causes instability. In general the available measurements in a vehicle active suspension system are the sprung mass acceleration, unsprung mass acceleration and suspension deflection. Therefore to implement a preview-active control system for the model defined by the state space Eqn (3.3), it is necessary to design an observer. Additionally the preview information must also be generated from the lead vehicle suspension response. The designed observer must:

- (i) Observe the states that cannot be measured from the available sensors
- (ii) Estimate the road profile from the vehicle and suspension response of any vehicle, whether lead or follower, with either passive, active or preview controlled suspension.

5.1 Observer design background

Let us consider a system given by (with noise added to the road)

$$\dot{x}(t) = Ax(t) + Bu(t) + F[z_r(t) + \xi(t)]$$

with the measurement equation

$$y = Cx(t) + v(t)$$

where $\xi(t)$ and $v(t)$ are the process and measurement noise respectively. For a stochastic system there might be presence of modeling uncertainties. These uncertainties may arise due to modeling errors such as neglecting nonlinear or higher frequency dynamics. This noise is generally called the process noise. The measurement noise is the random variation in the measurement and comes from the sensors used. An optimal Kalman estimator can be constructed following [33]

$$\dot{\hat{x}}(t) = A\hat{x}(t) + Bu(t) + \hat{L}(y - \hat{y}) \quad (5.1)$$

where

$$\hat{y} = C\hat{x}(t) + Du(t) \quad [D=0]$$

and \hat{L} is the optimal gain matrix given by

$$\hat{L} = \hat{P}C^T\bar{V}^{-1}$$

\hat{P} is the solution of the algebraic Riccati equation

$$A\hat{P} + \hat{P}A^T - \hat{P}C^T\bar{V}^{-1}C\hat{P} + FWF^T = 0$$

where $W = E\{\xi(t)\xi(t)^T\}$, $V = E\{v(t)v(t)^T\}$ are the process and measurement noise intensity matrices. The noises considered are white with zero mean, i.e., $E\{\xi(t)\} = E\{v(t)\} = 0$

5.2 Development of the proposed observer

Recall the quarter car model in Figure 3.1 with state space form given by Eqn (3.3),

$$\dot{x} = Ax + Bu + Fz_r$$

Let us define the measurement equation as

$$y = Cx + Du + Gz_r + v$$

$$\text{where } y = \begin{bmatrix} z_s - z_u \\ z_s \\ z_u \end{bmatrix} \text{ and } C = \begin{bmatrix} 1 & 0 & -1 & 0 \\ -\frac{k_s}{m_s} & -\frac{b_s}{m_s} & \frac{k_s}{m_s} & \frac{b_s}{m_s} \\ \frac{k_s}{m_u} & \frac{b_s}{m_u} & -\frac{(k_s+k_t)}{m_u} & -\frac{b_s}{m_u} \end{bmatrix}$$

$$D = \begin{bmatrix} 0 \\ \frac{1}{m_s} \\ -\frac{1}{m_u} \end{bmatrix} \text{ and } G = \begin{bmatrix} 0 \\ 0 \\ -\frac{k_t}{m_u} \end{bmatrix}$$

Let us reconstruct the observer including the unknown road profile as an input, as

$$\hat{\dot{x}} = A\hat{x} + Bu + F\hat{z}_r + \hat{L}(y - \hat{y})$$

and define the observed measurements as

$$\hat{y} = C\hat{x} + Du + G\hat{z}_r \quad (5.2)$$

The inclusion of road profile as an unknown input presents a challenge, as we wish to estimate road profiles for which no mathematical model can be assumed. Subtracting equation Eqn (3.1) from Eqn (3.2), we can write

$$m_s\ddot{z}_s + m_u\ddot{z}_u + k_t(z_u - z_r) = 0$$

Rewrite in terms of the road input:

$$z_r = z_u + \frac{m_s}{k_t}\ddot{z}_s + \frac{m_u}{k_t}\ddot{z}_u \quad (5.3)$$

and express the road profile in terms of observer states and measurements:

$$\hat{z}_r = \Delta\hat{x} + \Omega y \quad (5.4)$$

where $\Delta = \begin{bmatrix} 0 & 0 & 1 & 0 \end{bmatrix}$ and $\Omega = \begin{bmatrix} 0 & \frac{m_s}{k_t} & \frac{m_u}{k_t} \end{bmatrix}$. At any time, the road profile may be estimated by using Eqn (5.4) where unsprung mass deflection is one of the output states from the observer, and sprung and unsprung mass accelerations are the output measurements at that particular time. The intermediately estimated road profile can then be fed back into the observer model as an input. A schematic diagram is shown in Figure 5.1. Expanding the matrix equation of the observer gives

$$\dot{\hat{x}} = A\hat{x} + Bu + F\hat{z}_r + \hat{L}(y - C\hat{x} - Du - G\hat{z}_r) \quad (5.5)$$

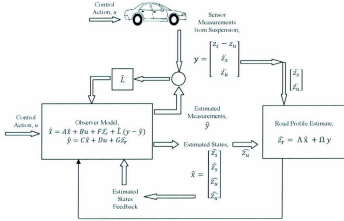


Figure 5.1: Schematic representation of the proposed observer

where \hat{z}_r is an estimate of the road input found from Eqn (5.4) and \hat{L} is the optimal gain matrix equal to

$$\hat{L} = (\hat{P}C^T + \bar{N})\bar{V}^{-1}$$

and \bar{P} is the solution of the algebraic Riccati equation. \bar{N} and \bar{V} are given by the following equations [31, 32],

$$\begin{aligned}\bar{V} &= V + GN + N^T G^T + GWG^T \\ \bar{N} &= F(WG^T + N)\end{aligned}$$

where

$$\begin{aligned}W &= E\{z_r(t)z_r(t)^T\} \\ V &= E\{v(t)v(t)^T\} \\ N &= E\{z_r(t)v(t)^T\}\end{aligned}$$

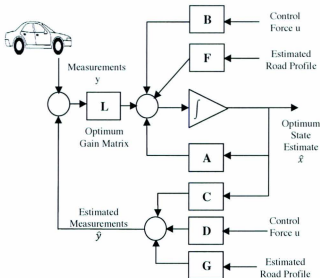


Figure 5.2: Block diagram of the observer

W and V are the process and measurement noise intensity matrices. The noises considered are white with zero mean, i.e., $E\{\xi(t)\} = E\{v(t)\} = 0$. The amplitude of the noise intensities are considered as in [10]. Though it has been considered that the road profile be a white noise process while designing the observer, the observer works well for other profiles as will be shown by simulation results. Figure 5.2 shows a representative block diagram of the proposed observer model. No integration or differentiation of the measurements is needed to generate the state estimates unlike many other methods in the literature [34, 10, 35]. Based on the observer model given by Eqn (5.5), (5.2) and (5.4) simulation has been carried out in MATLAB and the performance of the observer is shown below. The estimated road using this observer will be transferred to the follower vehicle to use as preview information. The road input considered is the same as in the previous section. Velocity of the vehicle for simulation is the same as in the previous section, i.e., 20 m/s with a preview time

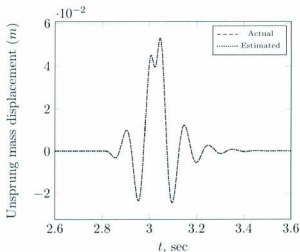


Figure 5.3: Actual vs. Estimated Wheel displacement (z_u) with preview(0.2s)

of 0.2 seconds. Figure 5.3 shows the estimated vs. actual sprung mass acceleration. Figure 5.4 and 5.5 shows the estimated tire and suspension deflection vs. the actual tire and suspension deflection. Figure 5.7 and 5.8 shows the estimated road profile vs. actual road profile for different types of road input.

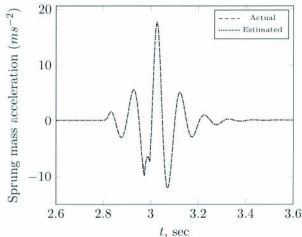


Figure 5.4: Actual vs. Estimated Sprung mass acceleration (z_s) with preview(0.2s)

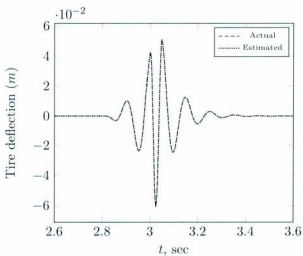


Figure 5.5: Actual vs. Estimated Tire deflection ($z_u - z_r$) with preview(0.2s)

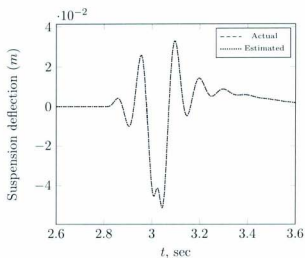


Figure 5.6: Actual vs. Estimated Suspension deflection ($z_s - z_u$) with preview(0.2s)

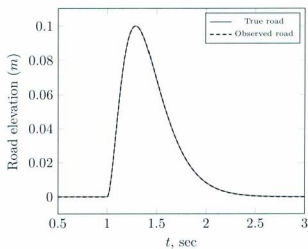


Figure 5.7: Road observation for the designed observer for rounded pulse

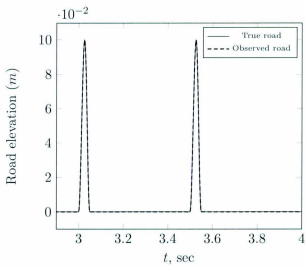


Figure 5.8: Road observation for the designed observer for two consecutive bumps

Chapter 6

Robust Convoy Preview with Active/Preview Switching

In this chapter the difficulties encountered by an ideal preview-controlled convoy system are discussed and the performance of the convoy-system is simulated for several realistic scenarios. Generally difficulties a convoy system working on preview may encounter could be due to

1. Faulty sensors in individual vehicles
2. Mid-convoy terrain changes
3. Communication error (preview information out of phase with road)

If the lead vehicle sensor is damaged, or if the lead vehicle hits a bump (thereby generating preview information for the followers) but dislodges it, then preview information will be incorrect. Performance of the followers' preview-controlled suspensions may be reduced significantly. This section simulates these situations and proposes a method to stop the propagation of error throughout the convoy system. Consider the following scenarios.

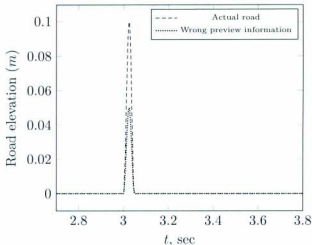


Figure 6.1: Incorrect road information generated by lead vehicle

6.1 Scenario 1: Presence of faulty sensors in lead vehicle

Consider the hypothetical case where the amplitude of the generated information from the lead vehicle is half of that of the actual road as shown in Figure 6.1. Figure 6.2 compares the resulting sprung mass accelerations of the follower vehicle. Figure 6.3-6.5 shows the unsprung mass deflection, suspension and tire deflection of the follower vehicle. Figure 6.2-6.5 show that the performance decreases in the presence of erroneous preview information.

6.2 Scenario 2: Mid-convoy terrain changes

Suppose the lead vehicle dislodges a bump. The follower vehicle expects to hit it but does not, and its preview controlled suspension reacts so the follower vehicle will

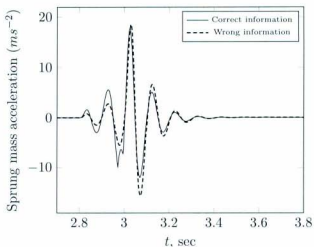


Figure 6.2: Ride quality (\dot{z}_s) of follower vehicle using correct and erroneous preview information

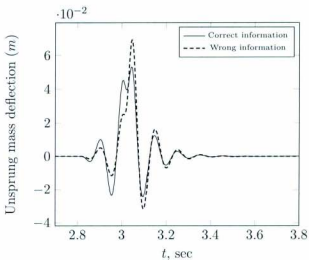


Figure 6.3: Unprung mass deflection (z_u) of follower vehicle using correct and erroneous preview information

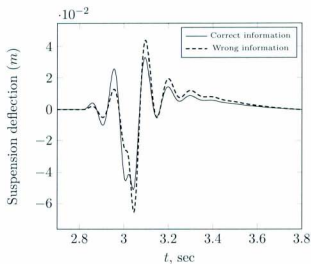


Figure 6.4: Suspension deflection ($z_s - z_u$) of follower vehicle using correct and erroneous preview information

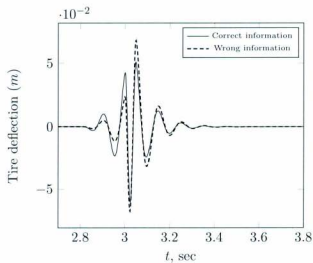


Figure 6.5: Tire deflection ($z_u - z_r$) of follower vehicle using correct and erroneous preview information

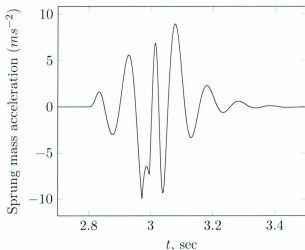


Figure 6.6: Ride quality (\ddot{z}_s) of follower vehicle due to spurious preview information (No actual bump)

undergo a transient response due to the spurious active suspension input. Figure 6.6-6.9 shows the responses due to the spurious information received by the preview controller of the follower vehicle.

6.3 Scenario 3: Lag/lead in the preview information

Suppose the lead vehicle can generate the preview information correctly but the information has a lag/lead when the first follower receives it.

6.3.1 Small time lag (0.005 sec)

Suppose the follower vehicle will hit the bump 0.005 seconds earlier than the calculated preview information. This can be depicted as in Figure 6.10,

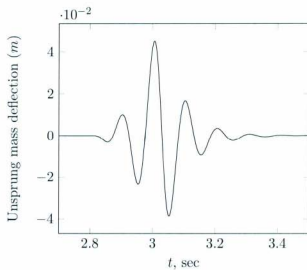


Figure 6.7: Unprung mass deflection (z_u) of follower vehicle due to spurious preview information (No actual bump)

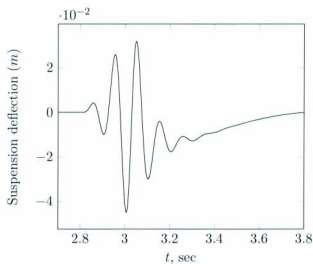


Figure 6.8: Suspension deflection ($z_s - z_u$) of follower vehicle due to spurious preview information (No actual bump)

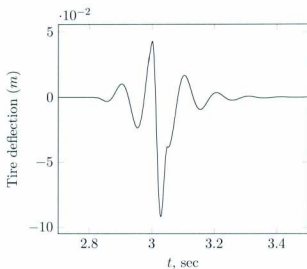


Figure 6.9: Tire deflection ($z_u - z_r$) of follower vehicle due to spurious preview information (No actual bump)

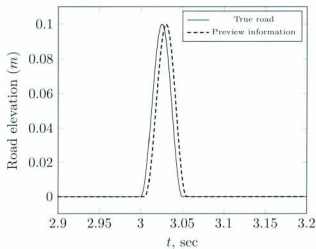


Figure 6.10: Preview information by the lead vehicle lagging by 0.005 seconds

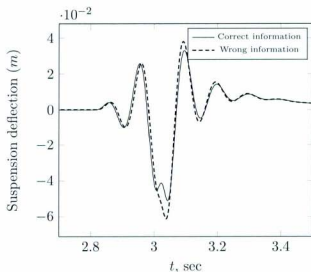


Figure 6.13: Suspension deflection ($z_s - z_u$) of follower vehicle due to small lag in preview information (lag time 0.005s)

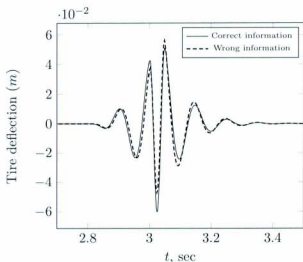


Figure 6.14: Tire deflection ($z_u - z_r$) of follower vehicle due to small lag in preview information (lag time 0.005s)

Figure 6.11-6.14 show the performance of the preview controller under this situation. Results show that the lag in the information by a small amount of time decreases the ride quality. Unsprung mass deflection increases by a small amount when the information is lagging (Figure 6.12). Minor reduction in road holding performance is noted for the positive peak but improvements in the negative peak can be observed (Figure 6.14). Deterioration in suspension deflection in both positive and negative peak can be observed from Figure 6.13.

6.3.2 Larger time lag (0.025 sec)

Let us consider that there is a relatively larger lag of 0.025 seconds as shown in Figure 6.15. Ride quality performance under this condition significantly decreases for the follower vehicle as can be observed from Figure 6.16. Figure 6.17 shows that the unsprung mass deflection has increased significantly unlike the performance when the lag is small. Road holding performance and suspension deflection has also decreased significantly when the lag is higher as shown in Figure 6.18 and 6.19.

6.3.3 Small lead time (0.005 sec)

Now consider that there is a small lead of 0.005 sec, i.e., the follower vehicle will hit the bump 0.005 sec later than the calculated preview information as shown in Figure 6.20. Figure 6.21-6.24 show the performance of the preview controller under this situation. Interestingly, the ride quality and road holding performance have been increased when the preview information is leading by a small amount of time. Suspension working space requirements remain the same as before and do not show any deterioration as shown in Figure 6.23. As for the unsprung mass displacement the performance is slightly increased because of the fact that the actuator reacts earlier and pulls the unsprung mass before it can hit the bump.

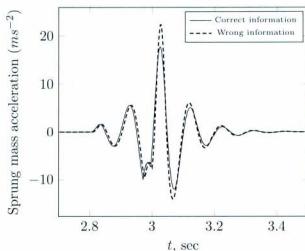


Figure 6.11: Ride quality (\dot{z}_s) of follower vehicle due to small lag in preview information (lag time 0.005s)

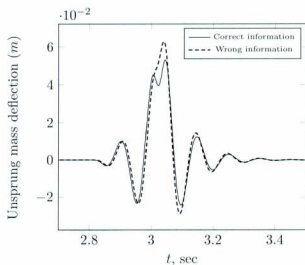


Figure 6.12: Unsprung mass deflection (z_u) of follower vehicle due to small lag in preview information (lag time 0.005s)

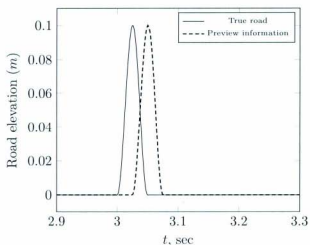


Figure 6.15: Preview information by the lead vehicle lagging by 0.025 seconds

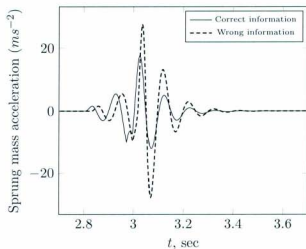


Figure 6.16: Ride quality (ε_s) of follower vehicle due to large lag in preview information (lag time 0.025s)

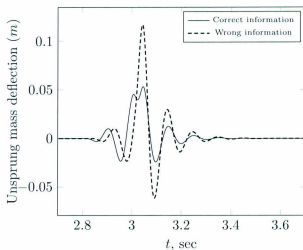


Figure 6.17: Unsprung mass deflection (z_u) of follower vehicle due to large lag in preview information (lag time 0.025s)

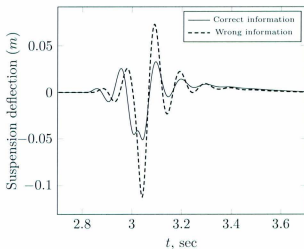


Figure 6.18: Suspension deflection ($z_s - z_u$) of follower vehicle due to large lag in preview information (lag time 0.025s)

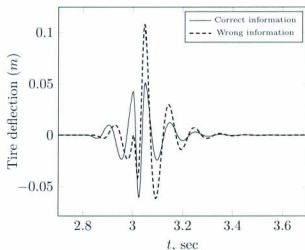


Figure 6.19: Tire deflection ($z_u - z_f$) of follower vehicle due to large lag in preview information (lag time 0.025s)

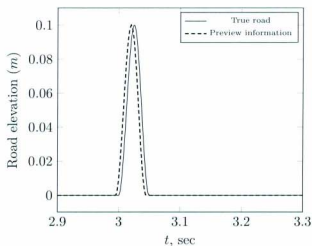


Figure 6.20: Preview information by the lead vehicle leading by 0.005 seconds

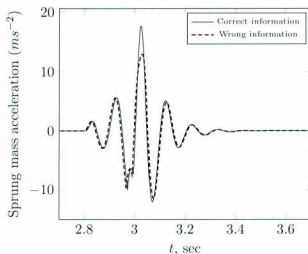


Figure 6.21: Ride quality (z_s) of follower vehicle due to small lead in preview information (lead time 0.005s)

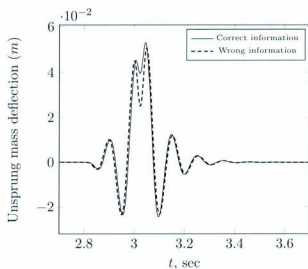


Figure 6.22: Unsprung mass deflection (z_u) of follower vehicle due to small lead in preview information (lead time 0.005s)

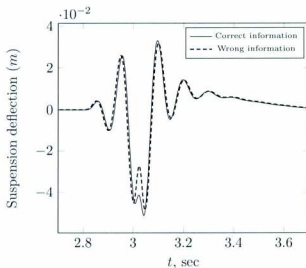


Figure 6.23: Suspension deflection ($z_s - z_u$) of follower vehicle due to small lead in preview information (lead time 0.005s)

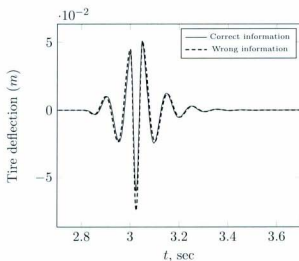


Figure 6.24: Tire deflection ($z_u - z_r$) of follower vehicle due to small lead in preview information (lead time 0.005s)

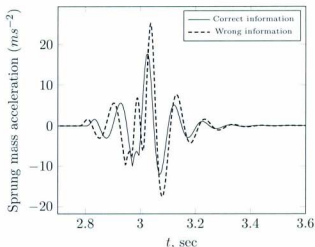


Figure 6.25: Ride quality (\bar{z}_s) of follower vehicle due to larger lead in preview information (lead time 0.025s)

6.3.4 Larger lead time (0.025 sec)

Performance of the follower vehicle under this situation can be observed from Figures 6.25-6.28. Ride quality and road holding performance degrade significantly. The suspension deflection is unchanged, and the unsprung mass deflection increases significantly. In summary, while the preview-controlled suspension is somewhat robust to small lead times in the receipt of preview information; the correct timing of the preview information is important and will be a practical challenge to the convoy preview suspension scheme proposed herein.

6.4 Convoy preview control

Given the implications of preview information error as described in the previous section, a means of preventing the error from propagating through the convoy is essential. This is feasible if each vehicle can estimate the road profile correctly even if its preview

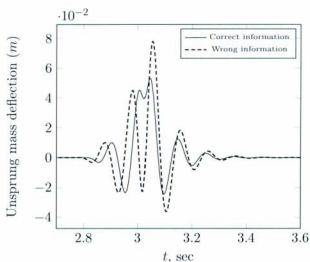


Figure 6.26: Unprung mass deflection (z_u) of follower vehicle due to larger lead in preview information (lead time 0.025s)

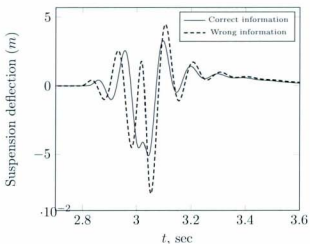


Figure 6.27: Suspension deflection ($z_s - z_u$) of follower vehicle due to larger lead in preview information (lead time 0.025s)

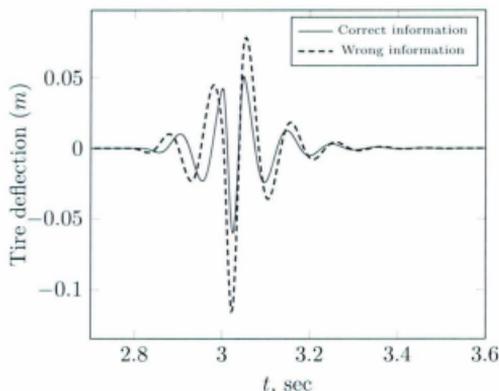


Figure 6.28: Tire deflection ($z_u - z_r$) of follower vehicle due to larger lead in preview information (lead time 0.025s)

information is erroneous. Erroneous information can be rejected using the following steps:

1. A vehicle's ongoing road profile estimation can be compared to recent preview information.
2. If comparison shows a large disparity then the vehicle could switch to a wheelbase preview system (outside the scope of this paper but the subject of ongoing work) where its front wheel would work in active mode and the rear wheel in preview mode.
3. For the next follower vehicle the correct information (estimated road profile) would be sent. If wheelbase preview is not available, the vehicle would switch to active control.
4. If the disparity of the estimation is not large then an average estimate of the

road profiles could be sent to the followers, thereby filtering out small errors from one vehicle.

This preview concept is shown in Figure 6.29. The proposed observer can estimate the road profile accurately even when the preview information is incorrect, making the concept shown above implementable. In each of the erroneous preview information cases discussed previously the observer estimates the true road very accurately. Estimated road profile by the observer for Scenario 1 (amplitude error) and scenario 2 (non-existent road event) are shown in Figures 6.30 and 6.31. When erroneous preview information is present then the propagation of error can be stopped immediately and the follower vehicle then can act as a lead vehicle.

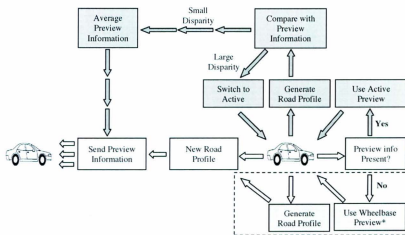


Figure 6.29: Concept of robust preview (*if available)

6.5 Preview-active to active switching

If the follower vehicle can change its control system from preview-active to active mode quickly enough, the effects of preview error can be minimized. Simulated re-

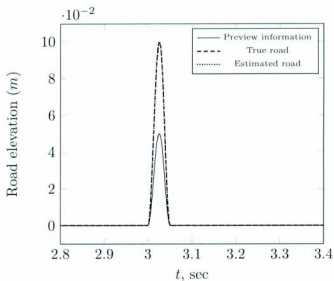


Figure 6.30: Estimated road profile by preview-controlled follower vehicle with incorrect preview information for Scenario 1

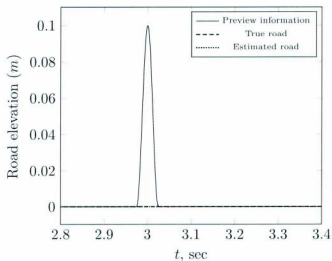


Figure 6.31: Estimated road profile by preview-controlled follower vehicle with incorrect preview information for Scenario 2

sults follow, with switching initiated when the discrepancy between the live estimate and preview information exceeds 2 cm. Figure 6.32-6.35 show the performance of the switched-suspension follower vehicle when working on an incorrect preview information. Road holding and unsprung mass deflection performance recover after switching to active suspension mode. Suspension deflection of the follower is increased by the switch to active mode.

6.6 Summary

To summarize, this switching method in conjunction with the proposed observer has the following benefits:

1. Follower vehicle can discard erroneous preview information from the lead vehicle and switch to active suspension or wheelbase preview mode to maximize performance
2. Follower vehicle can act as a lead vehicle thereby generating the correct preview information for the next follower vehicle and ceasing the propagation of the error throughout the convoy

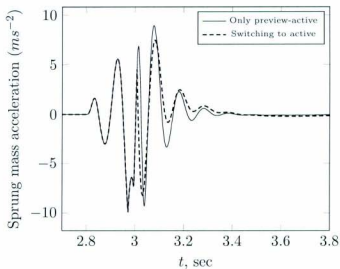


Figure 6.32: Ride quality (ε_s) of follower vehicle when switched from preview-active to active suspension mode

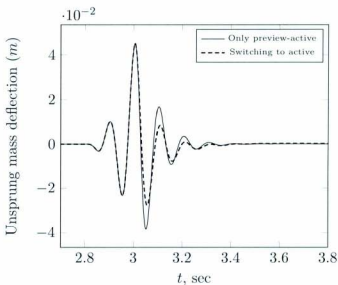


Figure 6.33: Unprung mass deflection (z_u) of follower vehicle when switched from preview-active to active suspension mode

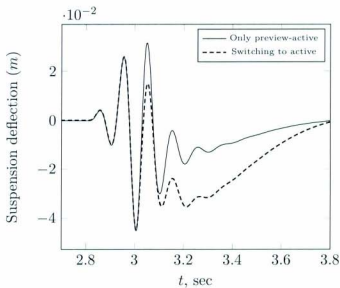


Figure 6.34: Suspension deflection ($z_s - z_u$) of follower vehicle when switched from preview-active to active suspension mode

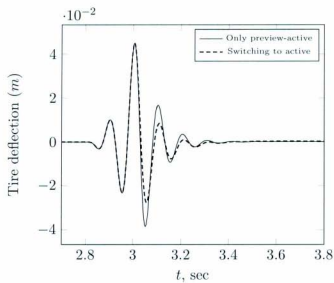


Figure 6.35: Tire deflection ($z_u - z_r$) of follower vehicle when switched from preview-active to active suspension mode

Chapter 7

Estimation Accuracy and Robustness of Observer for Actively Suspended Vehicle

In previous chapters we have shown that the preview-active suspension if applied in a convoy vehicle system can greatly enhance the performance of the suspension characteristics of the convoy system. A new and robust observer has been proposed and developed in the preceding chapter. The developed observer can estimate road profile irrespective of the suspension system present in the vehicle (i.e., active, preview-active or passive). But the accuracy of the estimated road profile depends on the performance of the observer and is susceptible to the measurement noise of the sensors (suspension sensors). The focus of the current chapter is to study the effect of the variation of measurement noise on estimation accuracy of any observer.

7.1 Motivation

Earlier studies of estimation accuracy of the observer have been done in [10] where a state observer is designed and the estimation accuracy is studied for the selection of measurement signals and loading conditions. [10] showed that the best estimation results from measuring suspension deflection, wheel velocity and body velocity. For the current study it is assumed that these three measurement signals are available. A state observer is designed for an actively suspended system and the observer performance is quantitatively assessed for different measurement noise level intensities unlike in [10] where the quantity of signal measurement is studied. Also the observer performance for different road noise level intensities are also assessed and the results are shown.

The rest of the chapter is organized as follows: the next section develops the quarter car model as in 3.1 and shows the development of feedback gains using the LQR method, followed by the development of the input road disturbance model. The deterministic model mimics road surface like traffic humps, railway crossings etc. Observer section 7.4 develops the observer followed by the simulation results, future works and conclusion.

7.2 System model

Consider the model shown in 3.1. This model can be effectively used to analyze the dynamic behavior in longitudinal and vertical directions. The justification is that the benefits of the active suspensions are primarily gained in these directions [34]. The equations of motion are given by (3.1) and (3.2). The determination of the optimal LQR gains are as follows,

The performance index for the LQR controller may be defined as in (4.1)

$$J = \lim_{T \rightarrow \infty} \frac{1}{2T} \int_0^T E[z_s^2 + \mu_1 \{z_s(t) - z_u(t)\}^2 + \mu_2 \{z_u(t) - z_r(t)\}^2 + \mu_3 u(t)^2] dt$$

where E is the expectation, and constants μ_x are the weighting parameters selected by the designer. (4.1) can be represented in matrix form upon substitution of (3.1) and (3.2),

$$J = \lim_{T \rightarrow \infty} \frac{1}{2T} \int_0^T E[x^T Q_1 x + 2x^T N u + u^T R u + 2x^T Q_{12} z_r + z_r^T Q_2 z_r] dt$$

where

$$Q_1 = \begin{bmatrix} \frac{k_x^2}{m_x^2} + \mu_1 & \frac{b_x k_x}{m_x^2} & -\frac{k_x^2}{m_x^2} - \mu_1 & -\frac{b_x k_x}{m_x^2} \\ \frac{b_x k_x}{m_x^2} & \frac{b_x^2}{m_x^2} & -\frac{b_x k_x}{m_x^2} & -\frac{b_x^2}{m_x^2} \\ -\frac{k_x^2}{m_x^2} - \mu_1 & -\frac{b_x k_x}{m_x^2} & \mu_1 + \mu_2 + \frac{k_x^2}{m_x^2} & \frac{b_x k_x}{m_x^2} \\ -\frac{b_x k_x}{m_x^2} & -\frac{b_x^2}{m_x^2} & \frac{b_x k_x}{m_x^2} & \frac{b_x^2}{m_x^2} \end{bmatrix}$$

$$R = \frac{1}{m_x^2} + \mu_3, \quad N = \begin{bmatrix} -\frac{k_x^2}{m_x^2} \\ -\frac{b_x}{m_x^2} \\ \frac{k_x^2}{m_x^2} \\ \frac{b_x}{m_x^2} \end{bmatrix}$$

and

$$Q_{12} = \begin{bmatrix} 0 & 0 & -\mu_2 & 0 \end{bmatrix}^T, \quad Q_2 = \mu_2$$

The last term of the performance index can be neglected because of the fact that the control input does not affect the road irregularities. So to minimize the expected

error in controlling the linear system given by equation (3.3) based on the separation theorem, the optimal control law is given by,

$$u = -\hat{G}\hat{x} \quad (7.1)$$

Where u is the control force in feedback form for the closed loop system \hat{x} is the output of the linear observer (optimal Kalman observer) and \hat{G} is the optimal solution given by [33]

$$\hat{G} = R^{-1}(B^T \hat{M} + N^T) \quad (7.2)$$

where \hat{M} is the solution to following algebraic Riccati equation [33]

$$0 = \hat{M}A_n + A_n^T \hat{M} - \hat{M}BR^{-1}B^T \hat{M} + Q_n \quad (7.3)$$

with $A_n = A - BR^{-1}N^T$ and $Q_n = Q1 - NR^{-1}N^T$.

7.3 Road disturbance input

Often a step function is used as a deterministic road surface in literature [4]. However, considering road inputs to be a step function is not realistic. Moreover Huisman [34] showed that, to demonstrate the performance capabilities of a suspension, a step function is not suitable and sometimes leads to erroneous conclusions. Rounded pulses are used by Alanoly and Sankar [36] and Marcelissen [37] to evaluate the suspension for incidental road disturbances. These rounded pulses can be described by

$$z_r = q_{max} \frac{e^2}{4} \left(\frac{2\pi t}{l_d}\right)^2 e^{(-\frac{2\pi t}{l_d})} \quad (7.4)$$

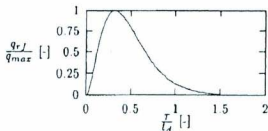


Figure 7.1: Rounded pulse

Where the height of the pulse is determined by q_{max} and l_d is a characteristic length such that the area under the pulse in the interval $[0, l_d]$ is approximately 95% of the total area (see Figure 7.3). The main advantage of these rounded pulses is that several road irregularities can be represented more or less by range of combinations of l_d and q_{max} [7].

7.4 Observer

For the full state feedback now we need to estimate the states \hat{x} using the observer. In this study a Kalman filter is used as an optimal estimator. We consider our system model as described by equation (3.3) with the measurement equation given by

$$y = Cx + v$$

where $C = \begin{bmatrix} 1 & 0 & -1 & 0 \\ 0 & 1 & 0 & 0 \\ 0 & 0 & 0 & 1 \end{bmatrix}$ and v is the measurement noise.

The Kalman observer model for the system can be expressed by the differential equation (see Figure 7.2)

$$\dot{\hat{x}} = A\hat{x} + Bu + \hat{L}(y - C\hat{x}) \quad (7.5)$$

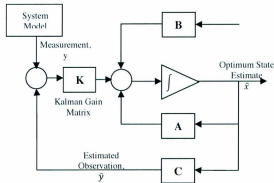


Figure 7.2: : Schematic Representation of Kalman observer block

where \hat{L} is the optimal Kalman observer gain matrix and is given by

$$\hat{L} == \hat{P}C^TV^{-1} \quad (7.6)$$

and \hat{P} is the solution of the algebraic Riccati equation

$$0 = A\hat{P} + \hat{P}A^T - \hat{P}C^TV^{-1}C\hat{P} + FWF^T$$

where $W = E\xi(t)\xi(t)^T$ and $V = Ev(t)v(t)^T$ are the process and measurement noise intensity matrices. The necessary and sufficient conditions for the existence of a positive, semi-definite solution for \hat{L} are that the pair $[A, F]$ is stabilizable and $[A, C]$ is detectable [38] which can easily be shown. Noise parameters for the current observer model are set as in [10], and the steady state optimal gain for the observer given by equation (7.6) is determined. The values are listed in the Appendix along with the Figure of the developed Simulink model. The input of the plant model is the control force for which the control law is derived using LQR method as described in earlier section. The output is the measurement matrix y . Noises are then added to the measurement matrix by the help of Simulink noise generator block.

7.5 Sensitivity to measurement noise

The primary objective of this study is to show the sensitivity of the designed observer when the measurement noise changes. The observer gain is generally calculated for a fixed measurement noise level and process noise level. Now if somehow the measurement noise changes (this happens in real life, sensors deteriorate over time) then it should be studied how much it affects the observer output because the gains are for a fixed noise to signal ratio and have not been changed. The observer gain has been determined for a prescribed noise level. Then the signal to noise ratio of the measurement is changed to show the effects on observer output. The changed measurement noises are listed in table 7.1.

Table 7.1: Measurement Noise Intensities for Simulation

Set	Noise for body velocity(σ_b^2)	Noise for suspension space(σ_s^2)	Noise for wheel velocity(σ_w^2)
1	1.6×10^{-6}	9.1×10^{-10}	3.6×10^{-5}
2	1.6×10^{-5}	9.1×10^{-9}	3.6×10^{-4}
3	1.6×10^{-4}	9.1×10^{-8}	3.6×10^{-3}
4	1.6×10^{-3}	9.1×10^{-7}	3.6×10^{-2}
5	1.6×10^{-2}	9.1×10^{-6}	3.6×10^{-1}

In this study it is assumed that the available measurements are sprung mass / body velocity (b.v), suspension working space (s.w.s) and unsprung mass / wheel mass velocity (w.v). An index is used to quantitatively assess the estimation accuracy of the observer. The index is taken as defined by [10] and can be expressed as

$$P_i = \left[1 - \frac{\sum_{k=1}^N [x_i(k) - \hat{x}_i(k)]^2}{\sum_{k=1}^N x_i^2(k)} \right] \times 100\% \quad (7.7)$$

here P_i is the performance index, i corresponds to the number of states and $k = 1, 2, 3, \dots, N =$ total number of sample points in simulation.

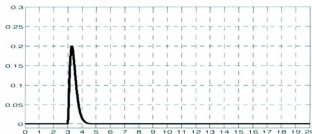


Figure 7.3: Deterministic Road Profile

7.6 Results

The study is carried out for the deterministic road signal (a rounded pulse starting from 3 seconds to 4.1 seconds approximately) with zero noise as in Figure 7.3. The input conditions and the measurement noise sets are shown in table 3.1 and table 7.1 respectively. Result shows that (Table 7.2) estimation accuracy for the unsprung/wheel mass velocity for set 4 and set 5, set 4 being the worst with performance index below 25% when the measurement noise intensities increases 100 times the initial value (set 4). For set 5, P_1 value of wheel velocity increases but the noise intensity for suspension working space and body velocity are increased 1000 times while the measurement noise for wheel velocity is kept constant (3.6×10^{-2}).

The implications are important suggesting interaction effects among the sensors and needs to be studied further. Estimation accuracy of sprung/body velocity, body displacement and unsprung/wheel mass displacement are good even if the measurement noise intensities are increased by 1000 times of the initial value and always remain above 98% except for the wheel displacement falling to 90% in the extreme scenario. The most important case for our study is the estimation accuracy of the road profile. Results show that the estimation accuracy falls below 90% when the noise intensities are increased to 100 times the initial value. Since it is of extreme importance that the

road profile estimation accuracy should be as high as possible for the use in preview active control and increase the quality of suspension, we can conclude that the noise intensity level must be kept within 0-10 times of the initial design value for good performance.

Table 7.2: Simulation Results for Deterministic Road

Estimation Accuracy Performance Index	Set 1	Set 2 (Design)	Set 3	Set 4	Set 5
P_1 for \dot{z}_s	100	100	100	99.99	100
P_2 for \dot{z}_u	99.87	99.18	92.27	23.60	55.52
P_3 for z_s	99.98	99.97	99.95	99.81	99.06
P_4 for z_u	99.80	99.74	99.49	98.09	90.06
P_5 for z_r	99.75	99.61	98.57	89.28	79.39

For the simplicity of assessment the output results for four representative sets has been given in Figure 7.4 in which 33038 simulation data points have been presented for each case. Each of the figures demonstrates the estimated value vs actual value (i.e., x vs \hat{x}) for each state variable.

7.7 Conclusion and future works

The main goal of the current study is to assess the estimation accuracy of the road profile for a designed observer with fixed weightings and parameters when the measurement noise intensity changes. The study shows that, to get a good estimation of the road profile the measurement noise intensity of the sensor must not be lower than 10 times the designed measurement noise intensity. The result is same for estimation of wheel velocity. Also it has been found that when the vehicle is subjected to rough road then for a good estimation accuracy the road roughness should not be increased beyond 10 times the designed road roughness. Beyond these levels the study shows

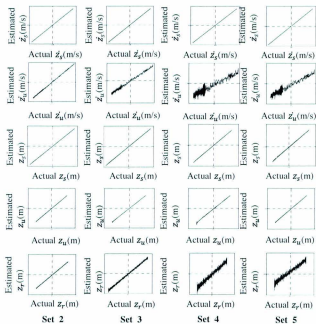


Figure 7.4: Estimated states vs. actual states for measurement noise variation (set 2-4). If estimated and actual data is same then the curve should be a 45 degree sharp straight line. Deviation from the line depicts estimation accuracy

the necessity of adaptive gain for the observer. The study also shows that there might be interaction effects between the sensor signals (when estimating the wheel velocity) which should be studied further. One possible solution might be to use a filter to reduce the noise levels of the measurement outputs before using them in the observer. But introduction of such a filter may affect the performance of the observer due to the dynamics of the filter itself. It is therefore necessary to study the effect of the filter dynamics on the performance of the observer.

Chapter 8

Optimal Preview Control of Convoy Vehicle Suspension: Half Car Model

The objective of this chapter is to establish an optimal preview control law for the follower vehicle in a convoy vehicle system as given by [2] using half car models. The road profile for the follower vehicle is generated by the lead vehicle based on its suspension response. In this chapter we will consider that the road profile is estimated by the lead vehicle and fed to the follower vehicle and develop the control law for the optimal preview control of the follower vehicle as shown in chapter 4.

8.1 Development of optimal control law

Consider the half car model shown in Figure 3.2. Equations of motion are given by Eqn (3.4) - (3.9). The corresponding state space form is given in Eqn (3.10) with the state space matrices α , β , and γ (Chapter 3). The optimal control problem is

to optimize the suspension system with respect to road holding, ride comfort and suspension working space. In addition, the magnitude of the control force must be constrained to the limits of the actuator. Defining the performance index as in [2] and expanding it for a half car model we get,

$$J = \lim_{\tau \rightarrow \infty} \frac{1}{2T} \int_0^T E[\mu_1 \dot{z}_{fc}^2 + \mu_2 \{z_{fc}(t) - z_{u_{fc}}(t)\}^2 + \mu_3 \{z_{u_{fc}}(t) - z_{r_f}(t)\}^2 + \mu_4 U_f(t)^2 + \mu_5 \dot{z}_{rc}^2 + \mu_6 \{z_{rc}(t) - z_{u_{rc}}(t)\}^2 + \mu_7 \{z_{u_{rc}}(t) - z_{r_r}(t)\}^2 + \mu_8 U_r(t)^2] dt \quad (8.1)$$

where E is the expectation, and constants μ_x are the weighting parameters selected by the designer. Eqn (8.1) can be represented in matrix form upon substitution of Eqn (3.8) and Eqn (3.9),

$$J = \lim_{\tau \rightarrow \infty} \frac{1}{2T} \int_0^T E[x^T Q_1 x + u^T R u + 2x^T N u + 2x^T Q_{12} z_r + z_r^T Q_2 z_r] dt \quad (8.2)$$

where

$$x(t) = \begin{bmatrix} z_{fc} & \dot{z}_{fc} & z_{u_{fc}} & \dot{z}_{u_{fc}} & z_{rc} & \dot{z}_{rc} & z_{u_{rc}} & \dot{z}_{u_{rc}} \end{bmatrix}^T$$

$$u(t) = \begin{bmatrix} U_f & U_r \end{bmatrix}^T$$

$$z_r(t) = \begin{bmatrix} z_{r_f} & z_{r_r} \end{bmatrix}^T$$

and Q_1 is defined as in Appendix A.

$$N = \begin{bmatrix} n_{11} & n_{12} \\ n_{21} & n_{22} \\ n_{31} & n_{32} \\ n_{41} & n_{42} \\ n_{51} & n_{52} \\ n_{61} & n_{62} \\ n_{71} & n_{72} \\ n_{81} & n_{82} \end{bmatrix} \quad R = \begin{bmatrix} r_{11} & r_{12} \\ r_{21} & r_{22} \end{bmatrix}$$

and

$$Q_{12} = \begin{bmatrix} 0 & 0 & -\mu_3 & 0 & 0 & 0 & 0 & 0 \\ 0 & 0 & 0 & 0 & 0 & 0 & -\mu_7 & 0 \end{bmatrix}^T$$

The last term of the performance index (Q_2) can be neglected because of the fact that the control input does not affect the road irregularities. The objective of linear optimal preview control is to find a control force, u so that the performance equation is minimized for an entire class of stochastic inputs $z_r(t)$. The control force $u(t)$ must contain a feedback term which takes the current states using optimal LQR theory and a feed-forward term from the knowledge of road ahead.

For the linear time invariant system given by Eqn (3.10) the measurement equation can be written as

$$y = \theta x + \zeta u + v \quad (8.3)$$

where v is the measurement noise from the sensors. Here the measured quantities are the states $x(t)$. Suppose the road profile is available up to time τ_p into the future, i.e., $z_r(\tau)$ is available where $\tau \in [t, t + \tau_p]$, and all the states at time t are present. Then the solution of the linear deterministic optimal preview control is given as [2]

$$u_o(t) = -R^{-1}[(N^T + \beta^T \bar{P})x(t) + \beta^T r(t)] \quad (8.4)$$

where \bar{P} is the solution of the algebraic Riccati equation given by

$$\bar{P}\alpha_n + \alpha_n^T\bar{P} + \bar{P}\beta R^{-1}\beta^T\bar{P} + Q_n = 0 \quad (8.5)$$

and the preview function is

$$r(t) = \int_0^{T_p} e^{\alpha_n^T\sigma} (\bar{P}\gamma + Q_{12})z_r(t + \sigma) d\sigma \quad (8.6)$$

where

$$\alpha_n = \alpha - \beta R^{-1}N^T \text{ and } Q_n = Q_1 - NR^{-1}N^T$$

The feedback part of Eqn (8.4) is

$$u_{ffo}(t) = -R^{-1}(N^T + \beta^T\bar{P})x(t) \quad (8.7)$$

The feedback gains can be found from the solution of the LQR problem that minimizes the performance index J. The feed-forward term is

$$u_{ffo}(t) = -R^{-1}\beta^T r(t) \quad (8.8)$$

The vector $r(t) \in \mathfrak{R}^n$ uses all the available future information about the road input z_r .

Eqn (8.7) and (8.8) are the continuous time optimal preview control law for the follower vehicle in a convoy vehicle system. At each step the preview control law requires the integration of the preview function given by Eqn (8.6) over the designed preview time. This requires higher simulation time. To improve simulation time the continuous preview function has been discretized by the use of exponential functions (see Appendix), and a variable shift register algorithm implemented, with discretization

done using MATLAB.

8.2 Discretization of Continuous System

Consider again the continuous system Eqn (3.10)

$$\dot{x}(t) = \alpha x(t) + \beta u(t) + \gamma z_r(t)$$

with measurements

$$y = \theta x(t) + \zeta u(t) + v(t)$$

where $v(t)$ is a white noise process with variance Q . We will consider the road profile to be an input to the system which is unknown at this point and will be estimated. The estimators will be optimal for random inputs, but we will also consider deterministic road inputs such as traffic humps, potholes, etc. The continuous system time response is given by [31, 32],

$$x(t) = e^{\alpha(t-t_0)}x(t_0) + \int_{t_0}^t e^{\alpha(t-\tau)}\beta u(\tau) d\tau + \int_{t_0}^t e^{\alpha(t-\tau)}\gamma z_r(\tau) d\tau \quad (8.9)$$

Let $t_0 = kT$, $t = (k+1)T$ for an integer k . Defining the sampled state function as $x_k \triangleq x(kT)$ we can write

$$x_{k+1} = e^{\alpha T}x_k + \int_{kT}^{(k+1)T} e^{\alpha[(k+1)T-\tau]}\beta u(\tau) d\tau + \int_{kT}^{(k+1)T} e^{\alpha[(k+1)T-\tau]}\gamma z_r(\tau) d\tau \quad (8.10)$$

Assuming that the control input $u(t)$ is reconstructed from the discrete control sequence u_k by using a zero order hold, and also that the unknown road input $z_r(t)$ is reconstructed from a discrete measurement sequence z_{rk} using a zero order hold, $u(\tau)$

and $z_r(\tau)$ have constant values of $u(kT) = u_k$ and $z_r(kT) = z_{rk}$ respectively over the integration interval. The discrete time equation becomes

$$x_{k+1} = e^{\alpha T} x_k + \int_{kT}^{(k+1)T} e^{\alpha[(k+1)T-\tau]} \beta d\tau \cdot u_k + \int_{kT}^{(k+1)T} e^{\alpha[(k+1)T-\tau]} \gamma d\tau \cdot z_{rk} \quad (8.11)$$

On changing the variables twice ($\lambda = \tau - kT$ and then $\tau = T - \lambda$) the above equation can be written as

$$x_{k+1} = e^{\alpha T} x_k + \int_0^T e^{\alpha \tau} \beta d\tau \cdot u_k + \int_0^T e^{\alpha \tau} \gamma d\tau \cdot z_{rk} \quad (8.12)$$

The equivalent discrete form of the system is then

$$x_{k+1} = \Phi_\alpha x_k + \Gamma_\beta u_k + \Psi_\gamma z_{rk} \quad (8.13)$$

where

$$\begin{aligned} \Phi_\alpha &= e^{\alpha T} = I + \alpha T + \frac{\alpha^2 T^2}{2!} + \dots \\ \Gamma_\beta &= \int_0^T e^{\alpha \tau} \beta d\tau = \beta T + \frac{\alpha \beta T^2}{2!} + \dots \\ \Psi_\gamma &= \int_0^T e^{\alpha \tau} \gamma d\tau = \gamma T + \frac{\alpha \gamma T^2}{2!} + \dots \end{aligned}$$

Discretization of the measurement equation is straightforward since it has no dynamics:

$$z_k = \theta x_k + \zeta u_k + v_k \quad (8.14)$$

The covariance \mathcal{R} of v_k in terms of the given covariance \mathcal{Q} can be found easily from

$$\mathcal{R} = \frac{\mathcal{Q}}{T}$$

For the current analysis the steady state LQR gains from the continuous system are used for the feedback part of the actuator force given by Eqn (8.7). The feed-forward part given by Eqn (8.8) contains the preview function

$$r(t) = \int_0^{T_p} e^{\alpha_c T \sigma} (\bar{P}\gamma + Q_{12}) z_r(t + \sigma) d\sigma$$

This must also be discretized. The discrete preview function at any step can be found from the preview function value calculated at the previous step and is given by (see Appendix)

$$r_{k+1} = \mathcal{F}^{-1} r_k - \mathcal{F}^{-1} z_{r_k} \mathcal{M} \Delta t + \mathcal{F}^n z_{r_{k+n+1}} \mathcal{M} \Delta t \quad (8.15)$$

where

$$\mathcal{F} = e^{\alpha_c T \Delta t}$$

$$\mathcal{M} = \bar{P}\gamma + Q_{12}, \quad T_p = n\Delta t$$

Here Δt can be the same as the discretization time step T . A more general form of the preview function calculation (variable shift register approach) can be written as Eqn (4.16). where the preview information at r_{k+p} is to be determined given that the preview information at r_{k-q} is known and

$$S_1 = \sum_{i=p+q,j=0}^{1,p+q-1} \mathcal{F}^{-i} z_{r_{k-q+j}} \mathcal{M} \Delta t$$

$$S_2 = \sum_{i=p+q,j=0}^{1,p+q-1} \mathcal{F}^{n-i+1} z_{r_{k+n+j}} \mathcal{M} \Delta t$$

where $p + q < n$.

8.3 Simulation results

Simulation is carried out using MATLAB for the scenario where the follower vehicle receives the preview information, i.e., the road profile, from the lead vehicle. Vehicle parameters are listed in table 3.2 on page 21. The road input considered here is a single half-sinusoidal bump expressed using the following equation [2],

$$Road(t) = \begin{cases} c[1 - \cos 40\pi(t - 3)], & t \in [3, 3.05] \\ 0, & \text{otherwise} \end{cases}$$

where $2c$ is the height of the bump in meters and t is the time in seconds. A bump height of 10 cm has been considered for simulation with vehicle velocity 20 m/s . Since the road input at rear wheel will be the same as front wheel the matrix $z_r(t)$ can be written as

$$z_r(t) = \begin{bmatrix} z_{r_f}(t) \\ z_{r_f}(t - \delta t) \end{bmatrix}$$

and $z_{r_f}(t) = Road(t)$ with $\delta t = \frac{V_f}{l}$
 where $V_f =$ vehicle velocity and $l = l_f + l_r$.

8.3.1 Road holding weighting factors

Simulation results are shown in this section for the optimal half car gains found using weighting factors which put more emphasis on road holding than ride comfort. For active and preview active suspension the weights of the performance index are $\mu_1 = 1$, $\mu_2 = 10^3$, $\mu_3 = 10^5$, $\mu_4 = 0$, $\mu_5 = 1$, $\mu_6 = 10^3$, $\mu_7 = 10^5$ and $\mu_8 = 0$. Figure 8.1 shows the vertical acceleration of the vehicle body at front corner $z_{f_c}^{\sim}$ for preview and passive systems. Figure 8.2 shows the vertical acceleration of the vehicle body at the rear corner $z_{r_c}^{\sim}$ for passive and preview active suspension. The force actuator has been saturated by clipping the force at $\pm 4000N$, i.e., $u \in [-4000N, 4000N]$. A preview time of 0.28 seconds has been used. Figures 8.3 and 8.4 show the front and rear tire deflection $((z_{u_{f_c}} - z_{r_f})$ and $(z_{u_{r_c}} - z_{r_r}))$. Figure 8.5 and 8.6 shows the suspension deflection of vehicle body at front and rear suspension respectively. Figure 8.7 shows the pitching acceleration of the vehicle body under the given road excitation for passive and preview active system. Only 9% improvement in the negative peak and a little deterioration in the positive peak has been observed. This is intuitive because we are putting more emphasis in road holding over ride comfort.

From the results it is evident that preview-active control is better compared to conventional passive suspension systems. Figure 8.3 and 8.4 shows better road tracking, with improvements of 13.26% and 17% in front and rear corner respectively compared to a passive system. Comparison of suspension deflection (Figure 8.5 and 8.6) shows 11.55% and 29.4% improvement over passive system in negative peaks. Large improvement in ride comfort have been observed from Figure 8.1 and 8.2 with 29% and 18% improvements at front and rear corner respectively with the chosen gain

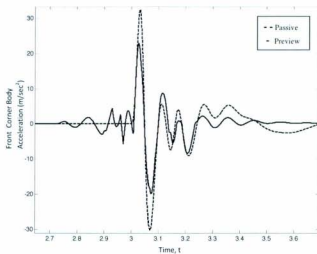


Figure 8.1: Front corner acceleration (z_{fc}^+) for Passive and Preview-active suspension system (Preview time 0.28 sec)

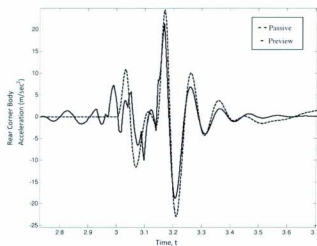


Figure 8.2: Rear corner acceleration (z_{rc}^-) for Passive and Preview-active suspension system (Preview time 0.28 sec)

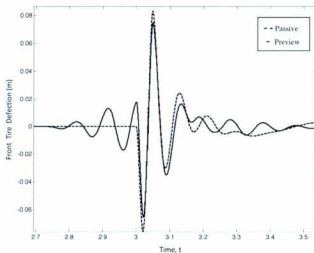


Figure 8.3: Front tire deflection ($z_{u_{fc}} - z_{r_f}$) for Passive and Preview-active suspension system (Preview time 0.28 sec)

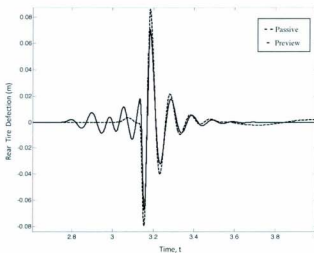


Figure 8.4: Rear tire deflection ($z_{u_{rc}} - z_{r_r}$) for Passive and Preview-active suspension system (Preview time 0.28 sec)

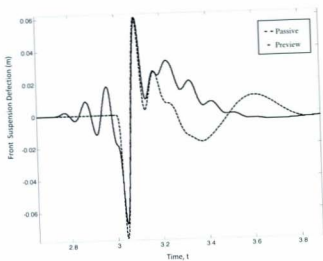


Figure 8.5: Front suspension deflection ($z_{fc} - z_{u_{fc}}$) for Passive and Preview-active suspension system (Preview time 0.28 sec)

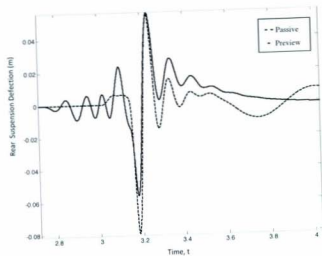


Figure 8.6: Rear suspension deflection ($z_{rc} - z_{u_{rc}}$) for Passive and Preview-active suspension system (Preview time 0.28 sec)

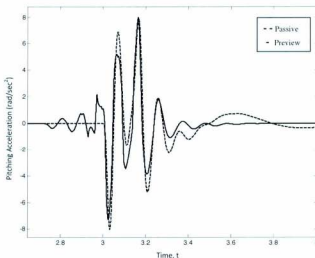


Figure 8.7: Pitching acceleration $\ddot{\theta}$ for Passive and Preview-active suspension system (Preview time 0.28 sec)

parameters emphasizing road holding.

8.3.2 Ride quality weighting factors

Weighting factors that put more emphasis on ride comfort have also been considered for simulation: $\mu_1 = 1$, $\mu_2 = 0.5$, $\mu_3 = 10^4$, $\mu_4 = 0.000001$, $\mu_5 = 1$, $\mu_6 = 0.5$, $\mu_7 = 10^4$ and $\mu_8 = 0.000001$. Results are shown in Figure 8.8-8.12.

From the results it is evident that preview-active control is better compared to conventional passive suspension systems with half car model. Figures 8.10 and 8.11 shows better road tracking, with improvements of 9% and 9% in front and rear corner respectively compared to a passive system but is smaller compared to what we found for road holding gains. This is reasonable because we are putting more emphasis on ride quality. Significantly large improvement in ride comfort have been observed from Figure 8.8 and 8.9 with 35% and 46% improvements at front and rear corner

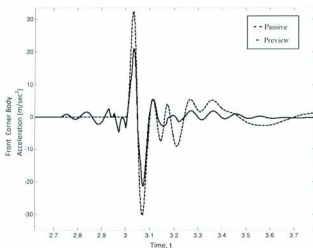


Figure 8.8: Front corner acceleration (z''_{f_c}) for Passive and Preview-active suspension system for ride comfort (Preview time 0.28 sec)

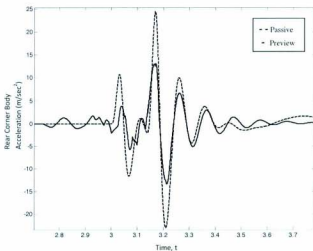


Figure 8.9: Rear corner acceleration (z''_{r_c}) for Passive and Preview-active suspension system for ride comfort (Preview time 0.28 sec)

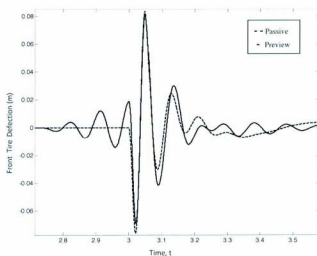


Figure 8.10: Front tire deflection ($z_{u_f} - z_{r_f}$) for Passive and Preview-active suspension system for ride comfort (Preview time 0.28 sec)

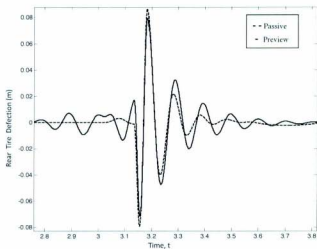


Figure 8.11: Rear tire deflection ($z_{u_{re}} - z_{r_r}$) for Passive and Preview-active suspension system for ride comfort (Preview time 0.28 sec)

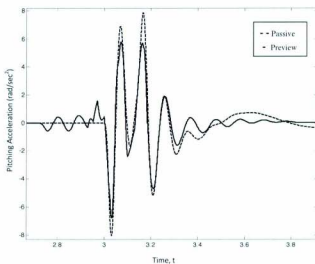


Figure 8.12: Pitching acceleration $\ddot{\theta}$ for Passive and Preview-active suspension system for ride comfort (Preview time 0.28 sec)

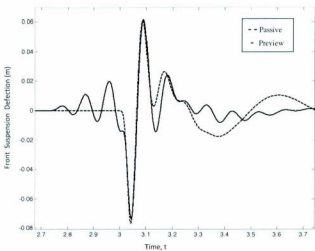


Figure 8.13: Front suspension deflection ($z_{u_{f_s}} - z_{r_f}$) for Passive and Preview-active suspension system for ride comfort (Preview time 0.28 sec)

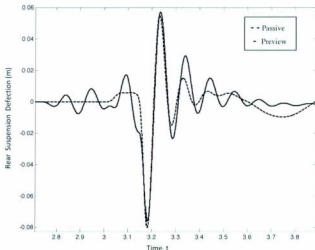


Figure 8.14: Rear suspension deflection ($z_{u_{rv}} - z_{r_e}$) for Passive and Preview-active suspension system for ride comfort (Preview time 0.28 sec)

respectively with the chosen gain parameters emphasizing ride comfort. Comparison of suspension deflection (Figure 8.13 and 8.14) shows a little deterioration with 1% and 4% decrease in performance in the positive peak but 3% and 5% improvement in the negative peak. It should also be noted that suspension deflection comes to steady state quickly. Figure 8.12 compares the pitching acceleration ($\ddot{\theta}$) of passive and preview active suspension system and shows major improvement with 26.35% and 15.83% in positive and negative peaks respectively. It should be noted that the improvements using quarter car model with quarter car algorithm is more impressive than half car model with half car controllers. Study must also be done for a half car model with quarter car control algorithms to compare the results and to find if quarter car algorithm works better than a half car algorithm or not.

The method of current research allows preview information from different possible lead vehicles to be used, allowing preview time to be varied in an actual implementation. Different forward speeds will have different optimal preview times, again motivating

the departure from fixed look-ahead sensors for which a single preview time is associated with a given vehicle velocity. It has also been found in our simulations that there exists a trend in the performance improvement such that if the vehicle speed is increased over a limited range for the same single bump, then preview suspension performance increases.

Chapter 9

Conclusion

9.1 Summary

In this thesis a new approach to preview control of convoy vehicles has been presented. Rather than use potentially unreliable look-ahead sensors that restrict preview time, the proposed method uses the responses of lead vehicles to estimate the road profile and generate preview information thereby. A new vehicle state observer has been designed, in which the road profile is accurately estimated despite being an unknown disturbance with no assumed mathematical description. Discrete bumps are estimated very accurately, and it is such bumps for which preview suspension is anticipated to have the most practical benefit. The observer requires three practically available measurements: sprung mass acceleration, unsprung mass acceleration, and suspension deflection. No differentiation or integration of the measurements is required. The preview control has been implemented for linear quarter car and half car models using a computationally efficient discrete time formulation, with the preview function computed using a shift-register approach. Preview control gave significant improvements over active suspension in terms of ride quality and roadholding. Challenging

aspects of convoy preview are timely communication of preview information, possible suspension sensor malfunction, and mid-convoy terrain changes due to dislodged obstacles or path variation. Simulation results show some robustness to small errors in preview information communication timing, especially when preview information leads the actual bump. The proposed observer can estimate the road profile very accurately even in the presence of incorrect preview information from the preceding vehicle. As a result of each vehicle being able to perform its own road estimation and compare it to preview information, its suspension can be switched from preview to conventional active control if discrepancies are significant. Preview errors can therefore be attenuated and not passed back through the entire string of vehicles. Contributions of the current work can be listed as follows,

1. MATLAB implementation of a computationally efficient discrete time preview controller. Such a controller may be useful for applications other than vehicle suspension control.
2. A robust road profile estimator which uses easily measured vehicle responses to reconstruct road profiles.
3. A scheme for assessing the correctness of preview information received by a given vehicle. This allows the detection of faulty sensors or changes in terrain from one vehicle to the next.

Overall this thesis work demonstrates the feasibility of using lead vehicle responses to generate preview information, rather than using terrain sensors on each vehicle. This could someday improve the driver comfort and safety using existing active suspension technology and emerging vehicle to vehicle communication protocols.

9.2 Future works

Future work will implement the proposed observer in hardware using a quarter-car test bench. dSpace instrumentation may be used as a potential platform for a rapid control prototyping and testing of the proposed observer and control algorithm. A comparison of preview control algorithm for a half car model with quarter car algorithm may unveil the possibility of using less complex quarter car model algorithms in practice, reducing calculation time for hardware processors. Extension of the vehicle model to a full-car will allow use of wheelbase preview and will help to develop a combined controller for roll, pitch and heave. Full car models with lateral dynamics and driver models will be used to study robustness to path variation, which will be related to following distance. For the current study we considered linear model. Nonlinear model will be developed for future research works. While obvious applications of such convoy-preview control are military deployments and automated highway systems, future advances in vehicle-to-vehicle communication and global positioning system technology would make road preview from leading vehicles useful and accessible to the general motoring public.

Bibliography

- [1] D. Hrovat, *Applications of Optimal Control to advanced automotive Suspension Design*, ASME Journal of Dynamic Systems 115 (1993), pp. 328–342.
- [2] A. Hac, *Optimal Linear Preview Control of Active Vehicle Suspension*, *Vehicle System Dynamics*, Vehicle System Dynamics 21 (1992), pp. 167–195.
- [3] E. Bender, *Optimum Linear Preview Control with Application to Vehicle Suspension*, ASME Journal of Basic Engineering 100, pp. 213–221.
- [4] W. Foag and G. Grubel, *Multi-Criteria Control Design for Preview Vehicle Suspension Systems*, in *Proc. of the 10th IFAC World Congress on Automatic Control*, 1987.
- [5] N. Louam, D. Wilson, and R. Sharp, *Optimization and Performance Enhancement of Active Suspensions for Automobiles under Preview of the Road*, *Vehicle System Dynamics* 21 (1992), pp. 39–63.
- [6] J. Muijderland, *Preview-based control of suspensions systems for commercial vehicles*, *Vehicle System Dynamics* 32 (1999), pp. 237–247.
- [7] R. Huisman, F. Veldpaus, G.V. Heck, and J. Kok, *Preview Estimation and Control for (Semi)-Active Suspensions*, *Vehicle System Dynamics* 22 (1993), pp. 335–346.

- [8] C. Pilbeam and R. Sharp, *Performance potential and power consumption of slow-active suspension systems with preview*, *Ve* 25 (1996), pp. 169–183.
- [9] L.G. Rao and S. Narayanan, *Preview control of random response of a half car vehicle model traversing rough road*, *Journal of Sound and Vibration* 310 (2008), pp. 352–365.
- [10] F. Yu and D.A. Crolla, *State Observer Design for Adaptive Vehicle Suspension*, *Journal of Vehicle System Dynamics* 30 (1998), pp. 451–471.
- [11] F. Yu, J. Zhang, and D. Crolla, *A study of Kalman filter active vehicle suspension system using correlation of front and rear wheel inputs*, *Proceedings of the Institution of Mechanical Engineers, Part D: Journal of Automobile Engineering* 214 (2000), pp. 493–502.
- [12] H.A. asl and D. Rideout, *Using Lead Vehicle Response to Generate Preview Functions for Active Suspension of Convoy Vehicles*, in *Proc. of American Control Conference*, 2010.
- [13] H. Kim, H. Yang, and Y. Park, *Improving the vehicle performance with active suspension using road-sensing algorithm*, *Computers and Structures* 80 (2002), pp. 1569–1577.
- [14] J. Marzbanrad, G. Ahmadi, H. Zohoor, and Y. Hojjat, *Stochastic optimal preview control of a vehicle suspension*, *Journal of Sound and Vibration* 275 (2004), pp. 973–990.
- [15] A. Akbari and B. Lohmann, *Output feedback H_2/GH_2 preview control of active vehicle suspensions: a comparison study of LQG preview*, *Vehicle System Dynamics* 48 (2010), pp. 1475–1494.

- [16] S.N. R.S. Prabakar C. Sujatha, *Optimal semi-active preview control response of a half car vehicle model with magnetorheological damper*, Journal of Sound and Vibration 326 (2009), pp. 400-420.
- [17] L. Yan and L. Shaojun, *Preview control of an active vehicle suspension system based on a four-degree-of-freedom half-car model*, in *International Conference on Measuring Technology and Mechatronics Automation*, 2009.
- [18] M. Elmadany, B.A. Bassam, and A. Fayed, *Preview control of slow active suspension systems*, Journal of Vibration and Control 17 (2011), pp. 245-258.
- [19] R. Langlois and R. Anderson, *Preview control algorithms for the active suspension of an off-road vehicle*, Vehicle System Dynamics 24 (1995), pp. 65-97.
- [20] K. Kitching, D. Cebon, and D. Cole, *An Experimental Investigation of preview control*, Vehicle System Dynamics 32 (1999), pp. 459-478.
- [21] S. Nagiri, S. Doi, S. Shoh-no, and N. Hiraiwa, *Improvement of Ride comfort by preview vehicle suspension system*, SAE 917 (1992), pp. 81-87.
- [22] A. Vahidi and A. Eskandarian, *Influence of preview uncertainties in the preview control of vehicle suspensions*, Proceedings of the Institution of Mechanical Engineers, Part K: Journal of Multi-body Dynamics 216 (2002), pp. 295-301.
- [23] R. Langlois, D. Hanna, and R. Anderson, *Implementing preview control on an off-road vehicle with active suspension*, Vehicle System Dynamics 20 (1992), pp. 340-353.
- [24] A. Akbari, G. Koch, E. Pellegrini, S. Spirk, and B. Lohman, *Multi-objective preview control of active vehicle suspensions: Experimental results*, in *2nd International Conference on Advanced Computer Control*, 2010.

- [25] Y. Park and J. Stein, *Measurement signal selection and a simultaneous state and input observer*, Journal of Dynamic Systems, Measurement, and Control 110 (1988), pp. 166–173.
- [26] F. Yang and R. Wilde, *Observers for linear systems with unknown inputs*, IEEE Transactions on Automatic Control 33 (1988), pp. 677–681.
- [27] M. Hou and P. Miller, *Design of observers for linear systems with unknown inputs*, IEEE Transactions on Automatic Control 37 (1992), pp. 871–875.
- [28] S. Bhattacharyya, *Observer design for linear systems with unknown inputs*, IEEE Transactions on Automatic Control AC-23 (1978).
- [29] A. Alam, A. Gattami, and K. Johansson, *An experimental study on the fuel reduction potential of heavy duty vehicle platooning*, in *IEEE Annual Conference on Intelligent Transportation Systems*, 2010.
- [30] K. Wakeham and D. Rideout, *Model complexity requirements in design of half-car active suspension controllers*, in *Proc. of ASME dynamic systems and control conference*, 2011.
- [31] G. Franklin, J. Powell, and M. Workman *Digital Control of Dynamic Systems*, Addison-Wesley, 1990.
- [32] F. Lewis *Optimal Estimation*, John Wiley & Sons Inc, 1986.
- [33] B. Fireldand *Control System Design: An Introduction to State-Space Methods*, McGraw-Hill International, 1986.
- [34] R. Huisman, F. Veldpaus, H. Voets, and J. Kok, *An Optimal Continuous Time Control Strategy for Active Suspensions with Preview*, Ve 22 (1993), pp. 43–55.

- [35] H. Imine, Y. Delanne, and N. M. Sirdi, *Road Profile Input Estimation in Vehicle Dynamics Simulation*, *Vehicle System Dynamics* 44 (2006), pp. 285–303.
- [36] J. Alanoly and S. Sankar, *Semi-Active Force Generators for Shock Isolation*, *Journal of Sound and Vibration* 126 (1988), pp. 145–156.
- [37] A. P. M. Mercelessen, *Analysis of the pros and cons of the primary suspension system of a tractor-semitrailer excited by deterministic signals*, Eindhoven. University of Technology (1991).
- [38] K. Sharma, D.A. Crolla and D.A. Wilson *The design of a Fully active Suspension System Incorporating a Kalman Filter for State Estimation*, *International Conference on Control* 1 (1994), pp. 344–349.
- [39] D. Karnopp, *Active Damping in Road Vehicle Suspension Systems*, *Vehicle System Dynamics* 21 (1983), pp. 191–316.
- [40] R. Rajamani *Vehicle Dynamics and Control*, Springer, 2006.
- [41] D. Karnopp, *Research on Wheelbase Preview Control for Vehicle Semi-active Suspension Based on Neural Networks*, *Third International Symposium on Intelligent Information Technology Application* (2009), pp. 290–293.
- [42] A. Tewari *Modern Control Design with MATLAB and SIMULINK*, John Wiley and Sons, Ltd. , 2002.

Appendix A

Optimal Regulator Gain and the Riccati Equation

Consider the system,

$$\dot{x} = Ax + Bu + Fz_r$$

with measurement equation,

$$y = Cx + Du + Gz_r + v$$

The observer for the system is given by,

$$\begin{aligned}\dot{\hat{x}} &= A\hat{x} + Bu + F\hat{z}_r + \hat{L}(y - \hat{y}) \\ \hat{z}_r &= A\hat{z}_r + Bu + F\hat{z}_r + \hat{L}(y - C\hat{x} - Du - G\hat{z}_r)\end{aligned}$$

From above expressions we can write,

$$\dot{e} = \dot{x} - \dot{\hat{x}}$$

expanding the matrix equations,

$$\begin{aligned}
\hat{e} &= (A - LC)e + Fz_r - L(Du + Gz_r + v - Du - G\hat{z}_r) \\
&= (A - LC)e + Fz_r - LGz_r - Lv + LG\hat{z}_r \\
&= (A - LC)e + (F - LG)z_r + LG\hat{z}_r - Lv \\
&= (A - LC)e + \bar{F}z_r + LG\hat{z}_r - Lv \\
&= (A - LC)e + \bar{F}z_r + \bar{K}\hat{z}_r - Lv \\
&= (A - LC)e + \zeta
\end{aligned}$$

where $\bar{K} = LG$, $\bar{F} = F - LG$, and $\zeta = \bar{F}z_r + \bar{K}\hat{z}_r - Lv$. The objective is to minimize the square of the error. Now,

$$\begin{aligned}
E\{\zeta\zeta^T\} &= \bar{F}E\{z_r z_r^T\}\bar{F}^T + LE\{v v^T\}L^T - LE\{v \hat{z}_r^T\}\bar{K}^T - \bar{K}E\{\hat{z}_r v^T\}L^T + \bar{K}E\{\hat{z}_r \hat{z}_r^T\}\bar{K}^T \\
&= \bar{F}W\bar{F}^T + LVL^T - LX\bar{K}^T - \bar{K}X^T L^T + \bar{K}V\bar{K}^T \\
&= (F - LG)W(F - LG)^T + LVL^T - LX(LG)^T - LGX^T L^T + LGVG^T L^T \\
&= FWF^T - FWG^T L^T - LGWF^T + LGWG^T L^T + LVL^T - LXG^T L^T - LGX^T L^T + LVL^T \\
&= FWF^T + L(V + GWG^T + GVG^T - XG^T - GX^T)L^T - L\bar{W}^T F^T - F\bar{W}L^T \\
&= FWF^T + L\bar{V}L^T - L\bar{W}^T F^T - F\bar{W}L^T
\end{aligned}$$

where

$$\hat{V} = V + GWG^T + GVG^T - XG^T - GX^T$$

$$\bar{W} = WG^T W = E\{z_r(t)z_r(t)^T\}$$

$$V = E\{v(t)v(t)^T\}$$

$$X = E\{v(t)\hat{z}_r(t)^T\}$$

$$\mathcal{V} = E\{\hat{z}_r(t)\hat{z}_r(t)^T\}$$

Appendix B

Half Car LQR Matrices

Half car LQR matrices are given by

$$Q_1 = \begin{bmatrix} q_{11} & q_{12} & q_{13} & q_{14} & q_{15} & q_{16} & q_{17} & q_{18} \\ q_{21} & q_{22} & q_{23} & q_{24} & q_{25} & q_{26} & q_{27} & q_{28} \\ q_{31} & q_{32} & q_{33} & q_{34} & q_{35} & q_{36} & q_{37} & q_{38} \\ q_{41} & q_{42} & q_{43} & q_{44} & q_{45} & q_{46} & q_{47} & q_{48} \\ q_{51} & q_{52} & q_{53} & q_{54} & q_{55} & q_{56} & q_{57} & q_{58} \\ q_{61} & q_{62} & q_{63} & q_{64} & q_{65} & q_{66} & q_{67} & q_{68} \\ q_{71} & q_{72} & q_{73} & q_{74} & q_{75} & q_{76} & q_{77} & q_{78} \\ q_{81} & q_{82} & q_{83} & q_{84} & q_{85} & q_{86} & q_{87} & q_{88} \end{bmatrix}$$

here

$$q_{11} = \mu_2 + k_{f_s}^2 \mu_1 \pi_1^2 + k_{f_s}^2 \mu_5 \pi_2^2$$

$$q_{12} = b_{f_s} k_{f_s} \mu_1 \pi_1^2 + b_{f_s} k_{f_s} \mu_5 \pi_2^2$$

$$q_{13} = -\mu_2 - k_{f_s}^2 \mu_1 \pi_1^2 - k_{f_s}^2 \mu_5 \pi_2^2$$

$$q_{14} = -b_{f_s} k_{f_s} \mu_1 \pi_1^2 - b_{f_s} k_{f_s} \mu_5 \pi_2^2$$

$$q_{15} = k_{f_s} k_{r_s} \mu_1 \pi_1 \pi_2 + k_{f_s} k_{r_s} \mu_5 \pi_3 \pi_2$$

$$\begin{aligned}
q_{16} &= b_{rs}k_{fs}\mu_1\pi_1\pi_2 + b_{rs}k_{fs}\mu_5\pi_3\pi_2 \\
q_{17} &= -k_{fs}k_{rs}\mu_1\pi_1\pi_2 - k_{fs}k_{rs}\mu_5\pi_3\pi_2 \\
q_{18} &= -b_{rs}k_{fs}\mu_1\pi_1\pi_2 - b_{rs}k_{fs}\mu_5\pi_3\pi_2 \\
q_{21} &= b_{fs}k_{fs}\mu_1\pi_1^2 + b_{fs}k_{fs}\mu_5\pi_2^2 \\
q_{22} &= b_{fs}^2\mu_1\pi_1^2 + b_{fs}^2\mu_5\pi_2^2 \\
q_{23} &= -b_{fs}k_{fs}\mu_1\pi_1^2 - b_{fs}k_{fs}\mu_5\pi_2^2 \\
q_{24} &= -b_{fs}^2\mu_1\pi_1^2 - b_{fs}^2\mu_5\pi_2^2 \\
q_{25} &= b_{fs}k_{rs}\mu_1\pi_1\pi_2 + b_{fs}k_{rs}\mu_5\pi_3\pi_2 \\
q_{26} &= b_{fs}b_{rs}\mu_1\pi_1\pi_2 + b_{fs}b_{rs}\mu_5\pi_3\pi_2 \\
q_{27} &= -b_{fs}k_{rs}\mu_1\pi_1\pi_2 - b_{fs}k_{rs}\mu_5\pi_3\pi_2 \\
q_{28} &= -b_{fs}b_{rs}\mu_1\pi_1\pi_2 - b_{fs}b_{rs}\mu_5\pi_3\pi_2 \\
q_{31} &= -\mu_2 - k_{fs}^2\mu_1\pi_1^2 - k_{fs}^2\mu_5\pi_2^2 \\
q_{32} &= -b_{fs}k_{fs}\mu_1\pi_1^2 - b_{fs}k_{fs}\mu_5\pi_2^2 \\
q_{33} &= \mu_2 + \mu_3 + k_{fs}^2\mu_1\pi_1^2 + k_{fs}^2\mu_5\pi_2^2 \\
q_{34} &= b_{fs}k_{fs}\mu_1\pi_1^2 + b_{fs}k_{fs}\mu_5\pi_2^2 \\
q_{35} &= -k_{fs}k_{rs}\mu_1\pi_1\pi_2 - k_{fs}k_{rs}\mu_5\pi_3\pi_2 \\
q_{36} &= -b_{rs}k_{fs}\mu_1\pi_1\pi_2 - b_{rs}k_{fs}\mu_5\pi_3\pi_2 \\
q_{37} &= k_{fs}k_{rs}\mu_1\pi_1\pi_2 + k_{fs}k_{rs}\mu_5\pi_3\pi_2 \\
q_{38} &= b_{rs}k_{fs}\mu_1\pi_1\pi_2 + b_{rs}k_{fs}\mu_5\pi_3\pi_2 \\
q_{41} &= -b_{fs}k_{fs}\mu_1\pi_1^2 - b_{fs}k_{fs}\mu_5\pi_2^2 \\
q_{42} &= -b_{fs}^2\mu_1\pi_1^2 - b_{fs}^2\mu_5\pi_2^2 \\
q_{43} &= b_{fs}k_{fs}\mu_1\pi_1^2 + b_{fs}k_{fs}\mu_5\pi_2^2 \\
q_{44} &= b_{fs}^2\mu_1\pi_1^2 + b_{fs}^2\mu_5\pi_2^2 \\
q_{45} &= -b_{fs}k_{rs}\mu_1\pi_1\pi_2 - b_{fs}k_{rs}\mu_5\pi_3\pi_2 \\
q_{46} &= -b_{fs}b_{rs}\mu_1\pi_1\pi_2 - b_{fs}b_{rs}\mu_5\pi_3\pi_2 \\
q_{47} &= b_{fs}k_{rs}\mu_1\pi_1\pi_2 + b_{fs}k_{rs}\mu_5\pi_3\pi_2
\end{aligned}$$

$$\begin{aligned}
q_{48} &= b_{fs}b_{rs}\mu_1\pi_1\pi_2 + b_{fs}b_{rs}\mu_5\pi_3\pi_2 \\
q_{51} &= k_{fs}k_{rs}\mu_1\pi_1\pi_2 + k_{fs}k_{rs}\mu_5\pi_3\pi_2 \\
q_{52} &= b_{fs}k_{rs}\mu_1\pi_1\pi_2 + b_{fs}k_{rs}\mu_5\pi_3\pi_2 \\
q_{53} &= -k_{fs}k_{rs}\mu_1\pi_1\pi_2 - k_{fs}k_{rs}\mu_5\pi_3\pi_2 \\
q_{54} &= -b_{fs}k_{rs}\mu_1\pi_1\pi_2 - b_{fs}k_{rs}\mu_5\pi_3\pi_2 \\
q_{55} &= \mu_6 + k_{rs}^2 * \mu_5\pi_3^2 + k_{rs}^2\mu_1\pi_2^2 \\
q_{56} &= b_{rs}k_{rs}\mu_5\pi_3^2 + b_{rs}k_{rs}\mu_1\pi_2^2 \\
q_{57} &= -\mu_6 - k_{rs}^2\mu_5\pi_3^2 - k_{rs}^2\mu_1\pi_2^2 \\
q_{58} &= -b_{rs}k_{rs}\mu_5\pi_3^2 - b_{rs}k_{rs}\mu_1\pi_2^2 \\
q_{61} &= b_{rs}k_{fs}\mu_1\pi_1\pi_2 + b_{rs}k_{fs}\mu_5\pi_3\pi_2 \\
q_{62} &= b_{fs}b_{rs}\mu_1\pi_1\pi_2 + b_{fs}b_{rs}\mu_5\pi_3\pi_2 \\
q_{63} &= -b_{rs}k_{fs}\mu_1\pi_1\pi_2 - b_{rs}k_{fs}\mu_5\pi_3\pi_2 \\
q_{64} &= -b_{fs}b_{rs}\mu_1\pi_1\pi_2 - b_{fs}b_{rs}\mu_5\pi_3\pi_2 \\
q_{65} &= b_{rs}k_{rs}\mu_5\pi_3^2 + b_{rs}k_{rs}\mu_1\pi_2^2 \\
q_{66} &= b_{rs}^2\mu_5\pi_3^2 + b_{rs}^2\mu_1\pi_2^2 \\
q_{67} &= -b_{rs}k_{rs}\mu_5\pi_3^2 - b_{rs}k_{rs}\mu_1\pi_2^2 \\
q_{68} &= -b_{rs}^2\mu_5\pi_3^2 - b_{rs}^2\mu_1\pi_2^2 \\
q_{71} &= -k_{fs}k_{rs}\mu_1\pi_1\pi_2 - k_{fs}k_{rs}\mu_5\pi_3\pi_2 \\
q_{72} &= -b_{fs}k_{rs}\mu_1\pi_1\pi_2 - b_{fs}k_{rs}\mu_5\pi_3\pi_2 \\
q_{73} &= k_{fs}k_{rs}\mu_1\pi_1\pi_2 + k_{fs}k_{rs}\mu_5\pi_3\pi_2 \\
q_{74} &= b_{fs}k_{rs}\mu_1\pi_1\pi_2 + b_{fs}k_{rs}\mu_5\pi_3\pi_2 \\
q_{75} &= -\mu_6 - k_{rs}^2\mu_5\pi_3^2 - k_{rs}^2\mu_1\pi_2^2 \\
q_{76} &= -b_{rs}k_{rs}\mu_5\pi_3^2 - b_{rs}k_{rs}\mu_1\pi_2^2 \\
q_{77} &= \mu_6 + \mu_7 + k_{rs}^2\mu_5\pi_3^2 + k_{rs}^2\mu_1\pi_2^2 \\
q_{78} &= b_{rs}k_{rs}\mu_5\pi_3^2 + b_{rs}k_{rs}\mu_1\pi_2^2 \\
q_{81} &= -b_{rs}k_{fs}\mu_1\pi_1\pi_2 - b_{rs}k_{fs}\mu_5\pi_3\pi_2
\end{aligned}$$

$$q_{82} = -b_{fs}b_{rs}\mu_1\pi_1\pi_2 - b_{fs}b_{rs}\mu_5\pi_3\pi_2$$

$$q_{83} = b_{rs}k_{fs}\mu_1\pi_1\pi_2 + b_{rs}k_{fs}\mu_5\pi_3\pi_2$$

$$q_{84} = b_{fs}b_{rs}\mu_1\pi_1\pi_2 + b_{fs}b_{rs}\mu_5\pi_3\pi_2$$

$$q_{85} = -b_{rs}k_{rs}\mu_5\pi_3^2 - b_{rs}k_{rs}\mu_1\pi_2^2$$

$$q_{86} = -b_{rs}^2\mu_5\pi_3^2 - b_{rs}^2\mu_1\pi_2^2$$

$$q_{87} = b_{rs}k_{rs}\mu_5\pi_3^2 + b_{rs}k_{rs}\mu_1\pi_2^2$$

$$q_{88} = b_{rs}^2\mu_5\pi_3^2 + b_{rs}^2\mu_1\pi_2^2$$

$$N = \begin{bmatrix} n_{11} & n_{12} \\ n_{21} & n_{22} \\ n_{31} & n_{32} \\ n_{41} & n_{42} \\ n_{51} & n_{52} \\ n_{61} & n_{62} \\ n_{71} & n_{72} \\ n_{81} & n_{82} \end{bmatrix} \quad R = \begin{bmatrix} r_{11} & r_{12} \\ r_{21} & r_{22} \end{bmatrix}$$

here

$$n_{11} = -k_{fs}\mu_1\pi_1^2 - k_{fs}\mu_5\pi_2^2$$

$$n_{12} = -k_{fs}\mu_1\pi_1\pi_2 - k_{fs}\mu_5\pi_3\pi_2$$

$$n_{21} = -b_{fs}\mu_1\pi_1^2 - b_{fs}\mu_5\pi_2^2$$

$$n_{22} = -b_{fs}\mu_1\pi_1\pi_2 - b_{fs}\mu_5\pi_3\pi_2$$

$$n_{31} = k_{fs}\mu_1\pi_1^2 + k_{fs}\mu_5\pi_2^2$$

$$n_{32} = k_{fs}\mu_1\pi_1\pi_2 + k_{fs}\mu_5\pi_3\pi_2$$

$$n_{41} = b_{fs}\mu_1\pi_1^2 + b_{fs}\mu_5\pi_2^2$$

$$n_{42} = b_{fs}\mu_1\pi_1\pi_2 + b_{fs}\mu_5\pi_3\pi_2$$

$$n_{51} = -k_{rs}\mu_1\bar{\pi}_1\bar{\pi}_2 - k_{rs}\mu_5\bar{\pi}_3\bar{\pi}_2$$

$$n_{52} = -k_{rs}\mu_5\bar{\pi}_3^2 - k_{rs}\mu_1\bar{\pi}_2^2$$

$$n_{61} = -b_{rs}\mu_1\bar{\pi}_1\bar{\pi}_2 - b_{rs}\mu_5\bar{\pi}_3\bar{\pi}_2$$

$$n_{62} = -b_{rs}\mu_5\bar{\pi}_3^2 - b_{rs}\mu_1\bar{\pi}_2^2$$

$$n_{71} = k_{rs}\mu_1\bar{\pi}_1\bar{\pi}_2 + k_{rs}\mu_5\bar{\pi}_3\bar{\pi}_2$$

$$n_{72} = k_{rs}\mu_5\bar{\pi}_3^2 + k_{rs}\mu_1\bar{\pi}_2^2$$

$$n_{81} = b_{rs}\mu_1\bar{\pi}_1\bar{\pi}_2 + b_{rs}\mu_5\bar{\pi}_3\bar{\pi}_2$$

$$n_{82} = b_{rs}\mu_1\bar{\pi}_2^2 + b_{rs}\mu_5\bar{\pi}_3^2$$

and

$$r_{11} = \mu_4 + \mu_1\bar{\pi}_1^2 + \mu_5\bar{\pi}_2^2$$

$$r_{12} = \mu_1\bar{\pi}_1\bar{\pi}_2 + \mu_5\bar{\pi}_3\bar{\pi}_2$$

$$r_{21} = \mu_1\bar{\pi}_1\bar{\pi}_2 + \mu_5 * \bar{\pi}_3\bar{\pi}_2$$

$$r_{22} = \mu_8 + \mu_5\bar{\pi}_3^2 + \mu_1\bar{\pi}_2^2$$

Appendix C

Discretization of Preview Function (Shift-Register Approach)

The vector $r(t)$ is given by [2] as

$$r(t) = \int_0^{T_p} e^{A_c^T \sigma} (\bar{P}F + Q_{12}) z_r(t + \sigma) d\sigma \quad (\text{C.1})$$

In discrete form

$$r(t) = \sum_{i=0}^n e^{A_c^T i \Delta t} (\bar{P}F + Q_{12}) z_r(t + i \Delta t) \Delta t \quad (\text{C.2})$$

where $T_p = n \Delta t$. Letting, k be the current time index calculated from $k = \frac{t}{\Delta t}$, $\mathcal{F} = e^{A_c^T \Delta t}$ and $\mathcal{M} = \bar{P}F + Q_{12}$ we get

$$r(k) = \sum_{i=0}^n \mathcal{F}^i \mathcal{M} z_r(k + i) \Delta t \quad (\text{C.3})$$

Expanding

$$r(k) = [\mathcal{F}^0 z_r(k+0) + \mathcal{F}^1 z_r(k+1) + \dots + \mathcal{F}^{n-1} z_r(k+(n-1)) + \mathcal{F}^n z_r(k+n)] \mathcal{M} \Delta t \quad (\text{C.4})$$

At time index $k+1$,

$$r(k+1) = [\mathcal{F}^0 z_r[k+1] + \mathcal{F}^1 z_r(k+2) + \dots + \mathcal{F}^{n-1} z_r(k+n) + \mathcal{F}^n z_r(k+1+n)] \mathcal{M} \Delta t \quad (\text{C.5})$$

From (C.4) and (C.5) we can write

$$\frac{r(k)}{\mathcal{F} \mathcal{M} \Delta t} = \frac{r(k+1)}{\mathcal{M} \Delta t} - \mathcal{F}^n z_r(k+1+n) + \mathcal{F}^{-1} z_r(k)$$

re-arranging

$$r(k+1) = \mathcal{F}^{-1} r(k) - \mathcal{F}^{-1} z_r(k) \mathcal{M} \Delta t + \mathcal{F}^n z_r(k+n+1) \mathcal{M} \Delta t \quad (\text{C.6})$$

(C.6) shows the discrete value of the preview function at any time $t = (k+1)\Delta t$ given the preview value at previous time step. Similarly the value at any point of time $t = (k+2)\Delta t$ can be found easily given the value at any earlier point of time

$t = (k - 1)\Delta t$ as

$$\begin{aligned}
r(k+2) &= \mathcal{F}^{-3}r(k-1) - [\mathcal{F}^{-3}z_r(k-1) + \mathcal{F}^{-2}z_r(k) + \mathcal{F}^{-1}z_r(k+1)]\mathcal{M}\Delta t \\
&\quad + [\mathcal{F}^{n-2}z_r(k+n) + \mathcal{F}^{n-1}z_r(k+n+1) \\
&\quad \quad + \mathcal{F}^n z_r(k+n+2)]\mathcal{M}\Delta t \\
r(k+2) &= \mathcal{F}^{-3}r(k-1) - \sum_{i=3, j=0}^{1,2} \mathcal{F}^{-i}z_r(k-1+j)\mathcal{M}\Delta t \\
&\quad + \sum_{i=3, j=0}^{1,2} \mathcal{F}^{n-i+1}z_r(k+n+j)\mathcal{M}\Delta t
\end{aligned}$$

Similarly a more general form of the equation for the preview value at time $t = (k + p)\Delta t$ given the value of preview function at $t = (k - q)\Delta t$ can be written as

$$\begin{aligned}
r(k+p) &= \mathcal{F}^{-(p+q)}r(k-q) - \sum_{i=p+q, j=0}^{1, p+q-1} \mathcal{F}^{-i}z_r(k-q+j)\mathcal{M}\Delta t \\
&\quad + \sum_{i=p+q, j=0}^{1, p+q-1} \mathcal{F}^{n-i+1}z_r(k+n+j)\mathcal{M}\Delta t
\end{aligned}$$

Or

$$r(k+p) = \mathcal{F}^{-(p+q)}r(k-q) - S_1 + S_2 \quad (\text{C.7})$$

where

$$\begin{aligned}
S_1 &= \sum_{i=p+q, j=0}^{1, p+q-1} \mathcal{F}^{-i}z_r(k-q+j)\mathcal{M}\Delta t \\
S_2 &= \sum_{i=3, j=0}^{1, 2} \mathcal{F}^{n-i+1}z_r(k+n+j)\mathcal{M}\Delta t
\end{aligned}$$

and $p + q < n$

Appendix D

MATLAB Codes

Code File -1

%% Quarter Car Model (As in Hac 1992 [2])

global R NTplusBTP Ac PDplusQ12 tee ti tla A B D F C

%% Parameters

ms=250;
mu=45;
bs=1000;
bt=0;
ks=16000;
kt=160000;

% ms=400;
% mu=60;
% bs=1300;
% bt=0;
% ks=16000;
% kt=150000;

%% Cost Function

% zeddot^2 + p1(susp.def.)^2 + p2(tire def.^2) + p3(control force)^2
% Weighting factors - heavily weighted susp/tire deflection

p1=1e3;
p2=1e5;
p3=0;

% % Weighting factors - heavily weighted ride quality

% p1=0.5;
% p2=1e4;
% p3=0.000001;

%% State variables

ix1 = zS
ix2 = zsdot
ix3 = zu
ix4 = zsdot

% Matrix Form

% xdot = Ax + Eu + Fw
%

A=[0 1 0 0;
-ks/ms -bs/ms ks/ms bs/ms;
0 0 0 1;
ks/mu bs/mu -(ks+kt)/mu -bs/mu];

B=[0;
1/ms;
0;
-1/mu];

F=[0;
0;
0;

```

    kt/mu];

M=[0;
  -1;
  0;
  -1];

%% Measurements : Available Measurements from Actual System
% Matrix Form : y = Cx + Du + v, v=measurement noise

C=[1 0 -1 0;
  -ks/ms -bs/ms ks/ms bs/ms;
  ks/mu bs/mu -(ks+kt)/mu -bs/mu];

D=[0 0;
  1/ms 0;
  -1/mu kt/mu];

% E=[0;
%   -1;
%   -1];

%% LQR Gain Calculations Based on Cost Function Defined (See Above)
Q1 = [ks^2/ms^2+p1 bs*ks/ms^2 -ks^2/ms^2-p1 -bs*ks/ms^2;
      bs*ks/ms^2 bs^2/ms^2 -ks*bs/ms^2 -bs^2/ms^2;
      -ks^2/ms^2-p1 -ks*bs/ms^2 ks^2/ms^2+p1+p2 ks*bs/ms^2;
      -bs*ks/ms^2 -bs^2/ms^2 ks*bs/ms^2 bs^2/ms^2];

N = [-ks/ms^2;
      -bs/ms^2;
      ks/ms^2;
      bs/ms^2];

R = 1/ms^2+p3;

S = N; %should be N' (No problem if N or N')

Q2 = p2;
Q12 = [0;0;-p2;0];

%% Use Eq.(12)
[P,Lam,G]=care(A,B,Q1,R,S);
%P = unknown
%Lam = closed loop eigenvalues
%G = gain matrix

An = A - B*R^(-1)*N';
Ac = An - B*R^(-1)*B'*P;
PDplusQ12 = P*F+Q12;
minusAnTplusPBRB = -An'+P*B*R^(-1)*B';
NTplusBTP = N'+B'*P; % LQR gain Matrix
Klqr = (-1/R)*NTplusBTP;

```

```

% Calculation for Observer Gain (Not related to LQR Feedback Gain)
% Road Noise Covariance

W= 2*10^-4;

% Measurement Noise Covariance

V =[9.1*10^-9 0 0;
    0 1.6*10^-5 0;
    0 0 3.6*10^-3];

% Observer Gain Matrix

Nt=sqrt(9.1*10^-9+1.6*10^-5)*(sqrt(9.1*10^-9);sqrt(1.6*10^-5);sqrt(3.6*10^-3))';
Vbar=V+D(:,2)*W*D(:,2)'+D(:,2)*Nt+Nt'*D(:,2)';
Nbar=F*(W*D(:,2)'+Nt);

P=are(A',C'*Vbar^-1*C,F*W*F');
L=(P*C'+Nbar)*Vbar^-1;

```

Code File -2

```

%Discrete Solution for Passive, Active and Preview Active Q Car model
%Define The Discrete System

global R NTplusBTP Ac PDplusQ12 tee ti tla A B C F D road rt E n dt Ko
Actual_road

sysc=ss(A,[B F],C,[D(:,1) D(:,2)]);
syso=ss(A,[B L],C,0);

%Simulation Time Step (Discretization Time Step)
DT=0.00001;
usat=4000;

sysd=c2d(sysc,DT);
sysdo=c2d(syso,DT);
[Ad,Bd,Cd,Dd]=ssdata(sysd);
[Ao,Bo,Co,Do]=ssdata(sysdo);
Fd=Bd(:,2);
Bd=Bd(:,1);
Lo=Bo(:,2:end);
Bo=Bo(:,1);

C1=[1 0 0 0;
    0 1 0 0;
    0 0 1 0;
    0 0 0 1];

T=4.9;

u=0; % Force for Active-Preview with Suspension switching Capability

```

```

l=1;
tf=3.05;
ti=3;
c=0.05;

xp=zeros(4,T/DT);
xa=zeros(4,T/DT);
xpre=zeros(4,T/DT);
w=zeros(1,1+T/DT);

uactive=zeros(1,1+T/DT);
uprev=zeros(1,1+T/DT);

S1=[0 0 0 0]';
S2=[0 0 0 0]';
k=1;
kprev=0;
i=1;
j=1;

yp=zeros(4,T/DT);
ya=zeros(4,T/DT);
ypre=zeros(4,T/DT);

rdobs=zeros(1,T/DT);
rtstore=zeros(4,T/DT);

for t=0:DT:T

    % PREVIEW FUNCTION CALCULATION
    k=round(t/dt);

    for i=k-1:kprev+1
        S1=S1+(E^-j)*road(i)*PDplusQ12*dt;
        S2=S2+(E^(n-j+1))*road(round(n+i+1))*PDplusQ12*dt;
        j=j+1;
    end

    %Preview for the first step
    if (k == 0)
        rt(:,2)=rt(:,1);
    else
        rt(:,2)=(E^-(k-kprev))*rt(:,1)-S1+S2;
    end

    % Considers on rt value stabilization (zero in no bump Condition)
    if (abs(rt(:,2)-rt(:,1)) < 0.0000000001)
        rt(:,2)=0;
    end
end

```

```

%% ACTUATOR FORCE
ua= -(1/R)*((NTplusBTP)*xa(:,1));
upre= -(1/R)*((NTplusBTP)*xpre(:,1)+ B'*rt(:,2));

if upre>usat
    upre=usat;
elseif upre<=-usat;
    upre=-usat;
else
    upre;
end

if ua>usat
    ua=usat;
elseif ua<=-usat;
    ua=-usat;
else
    ua;
end

%% STATES CALCULATION (Active-Preview Switch)
xp(:,1+1)=Ad*xp(:,1)+Fd*Actual_road(k+1);
xa(:,1+1)=Ad*xa(:,1)+Bd*ua+Fd*Actual_road(k+1);
xpre(:,1+1)=Ad*xpre(:,1)+Bd*upre+Fd*Actual_road(k+1);

uactive(1)=ua;
uprev(1)=upre;

%% Measurements
yp=C1*xp(:,1+1);
ya=C1*xa(:,1+1);
ypre=C1*xpre(:,1+1);

%% Increment & Reset Integrating Variables
l=l+1;
kprev=k;
j=1;
S1=[0 0 0 0]';
S2=[0 0 0 0]';
rt(:,1)=rt(:,2);
end

%% PUBLISH DATA
t=0:DT:T;

for i=1:size(t,2)

```

```

    if ((t(i)) >= ti) && ((t(i)) <= tf)
        w(i) = 0.05*(1-cos(40*pi*(t(i))-ti));
    elseif ((t(i)) >= 1) && ((t(i)) <= 1.1)
        w(i) = 0*(1-cos(20*pi*(t(i))-1));
    elseif ((t(i)) >= 3.2) && ((t(i)) <= 3.3)
        w(i) = 0*(1-cos(20*pi*(t(i))-ti));
    elseif ((t(i)) >= 4) && ((t(i)) <= 4.1)
        w(i) = 0;
    else
        w(i) = 0;
    end
end

% Passive Suspension
zsdotp = xp(2,1:1+T/DT);
zudotp = xp(4,1:1+T/DT);
zsuspp = xp(1,1:1+T/DT)-xp(3,1:1+T/DT);
ztirep = xp(3,1:1+T/DT)-w(1:1+T/DT);
zup=xp(3,1:1+T/DT);
zsddotp=diff(zsdotp)./DT;
zuddotp=diff(zudotp)./DT;

% Active Suspension
zsdota = xa(2,1:1+T/DT);
zudota = xa(4,1:1+T/DT);
zsuspa = xa(1,1:1+T/DT)-xa(3,1:1+T/DT);
ztirea = xa(3,1:1+T/DT)-w(1:1+T/DT);
zua=xa(3,1:1+T/DT);
zsddota=diff(zsdota)./DT;
zuddota=diff(zudota)./DT;

% Preview-Active Suspension
zsdotpre = xpre(2,1:1+T/DT);
zudotpre = xpre(4,1:1+T/DT);
zsuspre = xpre(1,1:1+T/DT)-xpre(3,1:1+T/DT);
ztirepre = xpre(3,1:1+T/DT)-w(1:1+T/DT);
zupre=xpre(3,1:1+T/DT);
zsddotpre=diff(zsdotpre)./DT;
zuddotpre=diff(zudotpre)./DT;

efficiencyl(1)=(max(zsuspp)-max(zsuspre))/max(zsuspp)*100;
efficiencyl(2)=(min(zsuspre)-min(zsuspp))/min(zsuspp)*100;
efficiencyl(3)=(max(ztirep)-max(ztirepre))/max(ztirep)*100;
efficiencyl(4)=(min(ztirepre)-min(ztirep))/min(ztirep)*100;
efficiencyl(5)=(max(zsddotp)-max(zsddotpre))/max(zsddotp)*100;
efficiencyl(6)=(min(zsddotpre)-min(zsddotp))/min(zsddotp)*100;

efficiency(1)=(max(zsuspa)-max(zsuspre))/max(zsuspa)*100;
efficiency(2)=(min(zsuspre)-min(zsuspa))/min(zsuspa)*100;
efficiency(3)=(max(ztirea)-max(ztirepre))/max(ztirea)*100;
efficiency(4)=(min(ztirepre)-min(ztirea))/min(ztirea)*100;
efficiency(5)=(max(zsddota)-max(zsddotpre))/max(zsddota)*100;
efficiency(6)=(min(zsddotpre)-min(zsddota))/min(zsddota)*100;

```

```

effy=[efficiency1' efficiency']
%% Figures
figure;
plot(t(1:size(zsddotp,2)),zsddotp,'r',t(1:size(zsddota,2)),zsddota,'m',t(1:si
ze(zsddotpre,2)),zsddotpre,'--')
legend('Passive Suspension','Active Suspension','Preview Active
Suspension','Location','NorthEast')
ylabel('Sprung Mass Acceleration [m/s^2]')
xlabel('Time, t [sec]')
%%
figure;
plot(t(1:size(zsuspp,2)),zsuspp,'r',t(1:size(zsuspa,2)),zsuspa,'b',t(1:size(z
susppre,2)),zsusppre,'--')
legend('Passive Suspension','Active Suspension','Preview Active
Suspension','Location','NorthEast')
ylabel('Suspension Deflection [m]')
xlabel('Time, t [sec]')
%%
figure;
plot(t,w,'k',t(1:size(ztirep,2)),ztirep,'r',t(1:size(ztirea,2)),ztirea,t(1:si
ze(ztirepre,2)),ztirepre,'--')
legend('Road','Passive Suspension','Active Suspension','Preview Active
Suspension','Location','NorthEast')
ylabel('Tire Deflection [m]')
xlabel('Time, t [sec]')
%%
figure;
plot(t,uactive,'r',t,uprev)
ylabel('Actuator Force [N]')
xlabel('Time [sec]')

%%
figure;
plot(t,w,'k',t,xp(3,1:size(t,2)), 'r',t,xa(3,1:size(t,2)), 'm',t,xpre(3,1:size(
t,2)), '--')
legend('Road','Passive Suspension','Active Suspension','Preview Active
Suspension','Location','NorthEast')
ylabel('Unsprung Mass Displacement [m]')
xlabel('Time, t [sec]')

figure;
subplot(2,2,2)
plot(t,zsdot(1:size(t,2)), 'b')
ylabel('Sprung Mass Velocity [m/s]')
xlabel('Time [sec]')

subplot(2,2,3)
plot(t,ztire(1:size(t,2)), 'b')
ylabel('Tire Deflection, m')

```

```

xlabel('Time [sec]')

subplot(2,2,4)
plot(t,w,'b',t,x(3,1:size(t,2)),'r')
legend('Road','Unsprung Mass Displacement','location','NorthWest')

figure
subplot(3,1,1)
plot(t,Actual_road(1:size(t,2)))
axis([0 T -0.2 0.2])
legend('True Road, [m]')
subplot(3,1,2)
plot(t,road(1:size(t,2)))
axis([0 T -0.2 0.2])
legend('Preview Information, [m]')
subplot(3,1,3)
plot(t,rdots(1:size(t,2)))
axis([0 T -0.2 0.2])
legend('Observed Road, [m]')

l=[t' zsdot' zudot' zsusp' ztire' x(3,1:T/DT)'];
csvwrite('Preview_Data_2.dat',1,0,2);

figure
subplot(5,1,1)
plot(t,zsdot)
ylabel('Sprung Mass Velocity [m/s]')
xlabel('Time [sec]')

subplot(5,1,2)
plot(t,zudot)
ylabel('Unsprung Mass Velocity [m/s]')

subplot(5,1,3)
plot(t,w(1:1+T/DT),'b',t,x(3,1:1+T/DT),'r')
legend('Road','Unsprung Mass Displacement')
hold on

subplot(5,1,4)
plot(t,zsusp)
ylabel('Suspension Deflection [m]')

subplot(5,1,5)
plot(t,ztire)
ylabel('Tire Deflection [m]')

C33e File -3

%Discrete Solution for preview Active Q Car model with observer
%Define The Discrete System

global R NTplusBTP Ac PDplusQ12 tee ti tla A B C F D road rt E n dt Ko
Actual_road

```

```

sysc=ss(A,[B F],C,[D(:,1) D(:,2)]);
syso=ss(A,[B L],C,0);

%Simulation Time Step (Discretization Time Step)
DT=0.00001;

sysd=c2d(sysc,DT);
sysdo=c2d(syso,DT);
[Ad,Bd,Cd,Dd]=ssdata(sysd);
[Ao,Bo,Co,Do]=ssdata(sysdo);
Fd=Bd(:,2);
Bd=Bd(:,1);
Lo=Bo(:,2:end);
Bo=Bo(:,1);

T=4.9;

u=0; % Force for Active-Preview with Suspension switching Capability

l=1;
tf=3.1;
ti=3;
c=0.1;

x=zeros(4,T/DT);
xa=zeros(4,T/DT);
xn=zeros(4,T/DT);
w=zeros(1,1+T/DT);

S1=[0 0 0 0]';
S2=[0 0 0 0]';

k=1;
kprev=0;
i=1;
j=1;

yn1=zeros(3,T/DT);
yn=zeros(3,T/DT);
rdoBs=zeros(1,T/DT);
rtstore=zeros(4,T/DT);
ustore=zeros(1,1+T/DT);

for t=0:DT:T

    % k=ceil(t/dt) FUNCTION CALCULATION
    k=round(t/dt);

    for i=k:-1:kprev+1
        S1=S1+(E^-j)*road(i)*PDplusQ12*dt;
    end
end

```

```

        S2=S2+ (E^(n-j+1)) *road(n+1+1)*PDplusQ12*dt;
        j=j+1;
    end

%Preview for the first step
if (k == 0)
    rt(:,2)=rt(:,1);
else
    rt(:,2)=(E^-(k-kprev))*rt(:,1)-S1+S2;
end

% Condition on rt value stabilization (zero in no bump Condition)
if (abs(rt(:,2)-rt(:,1)) < 0.000000001)
    rt(:,2)=0;
end

% ACTUATOR FORCE

k      % (Active-Preview Switching)
%
%      if abs(road(k-1)-rdobs(1))>0.01
%          u = -(1/R)*(NTplusBTP)*xn(:,1);
%      else
%          u = -(1/R)*(NTplusBTP)*xn(:,1)+ B'*rt(:,2);
%      end

u = -(1/R)*(NTplusBTP)*xn(:,1)+ B'*rt(:,2);
ua = -(1/R)*(NTplusBTP)*xn(:,1);

%
%      if 1>1
%          if abs(road(k)-rdobs(1-1))>0.02
%              u = -(1/R)*(NTplusBTP)*xn(:,1)+ B'*rt(:,2);
%          else
%              u = -(1/R)*(NTplusBTP)*xn(:,1)+ B'*rt(:,2);
%          end
%      end

ustore(1)=u;
%      if u>=4000
%          u=4000;
%      end
%
%      if u<=-4000;
%          u=-4000;
%      end

% STATE CALCULATION (Active-Preview Switch)
x(:,1+1)=Ad*x(:,1)+Bd*u+Fd*Actual_road(k+1);
x(:,1+1)-Ad*x(:,1)+Bd*ua+Fd*Actual_road(k+1);
xn(:,1+1)=Ad*xn(:,1)+Bd*u+Lo*(yn(1,1)-yn(:,1))+Fd*rdobs(1);

```

```

% Measurements
yn1(:,1+1)=Cd*x(:,1+1)+Dd*[u;Actual_road(k+1)]+[sqrt(9.1*10^-
9).*randn();sqrt(1.6*10^-5).*randn();sqrt(3.6*10^-3).*randn()];

yn(:,1+1)=Cd*xn(:,1+1)+Dd*[u;xn(3,1)+(ms/kt)*yn1(2,1+1)+(mu/kt)*yn1(3,1+1)];

% Observed Road
rdobs(1+1)=xn(3,1)+(ms/kt)*yn1(2,1+1)+(mu/kt)*yn1(3,1+1);

% Increment & Reset Integrating Variables
l=l+1;
kprev=k;
j=1;
S1=[0 0 0 0]';
S2=[0 0 0 0]';
rt(:,1)=rt(:,2);
end

% PUBLISH DATA
t=0:DT:T;

for i=1:size(t,2)
    if ((t(i)) >= ti) && ((t(i)) <= tf)
        w(i) = 0.1*(1-cos(20*pi*((t(i))-ti)));
    elseif ((t(i)) >= 1) && ((t(i)) <= 1.1)
        w(i) = 0*(1-cos(20*pi*((t(i))-1)));
    elseif ((t(i)) >= 3.2) && ((t(i)) <= 3.3)
        w(i) = 0*(1-cos(20*pi*((t(i))-3.2)));
    elseif ((t(i)) >= 4) && ((t(i)) <= 4.1)
        w(i) = 0;
    else
        w(i) = 0;
    end
end

zsdot = x(2,1+1+T/DT);
zudot = x(4,1+1+T/DT);
zsusp = x(1,1+1+T/DT)-x(3,1+1+T/DT);
ztire = x(3,1+1+T/DT)-w(1+1+T/DT);
zu=x(3,1+1+T/DT);

Estim_zsdot = xn(2,1+1+T/DT);
Estim_zudot = xn(4,1+1+T/DT);
Estim_zsusp = xn(1,1+1+T/DT)-xn(3,1+1+T/DT);
Estim_ztire = xn(3,1+1+T/DT)-w(1+1+T/DT);

% zsdota = xn(2,1+1+T/DT);
% zudota = xn(4,1+1+T/DT);
% zsuspa = xn(1,1+1+T/DT)-xn(3,1+1+T/DT);
% ztirea = xn(3,1+1+T/DT)-w(1+1+T/DT);

zsddot=diff(zsdot)./DT;

```

```

zdddot=diff(zudot)./DT;
Estim_zsdddot=diff(Estim_zsdot)./DT;
% zsdgots=diff(zsdots)./DT;

%% Figures
figure
% subplot(2,2,1)
plot(t(1:size(zsddot,2)),zsddot,'r',t(1:size(zsddot,2)),Estim_zsddot,'b')
legend('Actual','Estimated','Location','NorthEast')
ylabel('Sprung Mass Acceleration [m/s^2]')
xlabel('Time [sec]')

% subplot(2,2,2)
% plot(t,zsdot(1:size(t,2)), 'b')
% ylabel('Sprung Mass Velocity [m/s]')
% xlabel('Time [sec]')
plot(t(1:size(zsusp,2)),zsusp,'r',t(1:size(zsusp,2)),Estim_zsusp,'b')
legend('Actual','Estimated','Location','NorthEast')
ylabel('Suspension Deflection, m')
xlabel('Time [sec]')
grid on

subplot(3,1,1)
plot(t(1:size(ztire,2)),ztire,'r',t(1:size(ztire,2)),Estim_ztire,'b')
legend('Actual','Estimated','Location','NorthEast')
ylabel('Tire Deflection, m')
xlabel('Time [sec]')
grid on

subplot(3,1,2)
% plot(L,w,'b',t,xn(3,1:size(t,2)), 'r')
% legend('Road','Unsprung Mass Displacement','Location','NorthEast')
% ylabel('Unsprung Mass Displacement, m')
% xlabel('Time [sec]')
% grid on
plot(t(1:size(zsddot,2)),zsddot,'r',t(1:size(zsddot,2)),Estim_zsddot,'b')
legend('Actual','Estimated','Location','NorthEast')
ylabel('Sprung Mass Acceleration [m/s^2]')
xlabel('Time [sec]')
grid on

subplot(3,1,3)
plot(t(1:size(zsusp,2)),zsusp,'r',t(1:size(zsusp,2)),Estim_zsusp,'b')
legend('Actual','Estimated','Location','NorthEast')
ylabel('Suspension Deflection, m')
xlabel('Time [sec]')
grid on

plot(t,Actual_road(1:size(t,2)), 'r',t,rdoabs(1:size(t,2)), 'b')
legend('Actual Road','Estimated Road','Location','NorthEast')
ylabel('Road Elevation, m')

```

```

xlabel('Time [sec]')
grid on

plot(t,Actual_road(1:size(t,2)), 'r',t, road(1:size(t,2)), 'b',t,rdots(1:size(t,
2)))
% axis([0 T -0.2 0.2])
legend('True Road [m]', 'Preview Information [m]', 'Estimated Road [m]')
ylabel('Road Elevation, m')
xlabel('Time [sec]')
grid on

figure
% subplot(3,1,1)
plot(t,Actual_road(1:size(t,2)), 'r',t, road(1:size(t,2)), 'b')
axis([0 T -0.2 0.2])
legend('Actual Road, [m]', 'Preview Information, [m]')

subplot(3,1,2)
plot(t, road(1:size(t,2)))
axis([0 T -0.2 0.2])
legend('Preview Information, [m]')
subplot(3,1,3)
plot(t, rdots(1:size(t,2)))
axis([0 T -0.2 0.2])
legend('Observed Road, [m]')
grid on

l=[t' zsdot' zudot' z susp' ztire' x(3,1:1+T/DT)'];
csvwrite('Preview_Data_z.dat',1,0,2);

figure
subplot(5,1,1)
plot(t,zsdot)
ylabel('Sprung Mass Velocity [m/s]')
xlabel('Time [sec]')

subplot(5,1,2)
plot(t,zudot)
ylabel('Unsprung Mass Velocity [m/s]')

subplot(5,1,3)
plot(t,w(1:1+T/DT), 'b',t,x(3,1:1+T/DT), 'r')
legend('Road', 'Unsprung Mass Displacement')
hold on

subplot(5,1,4)
plot(t,z susp)
ylabel('Suspension Deflection [m]')

```

```
subplot(5,1,5)
plot(t,ztire)
ylabel('Tire Deflection [m]')

% End of codes
```

Appendix E

SIMULINK Models

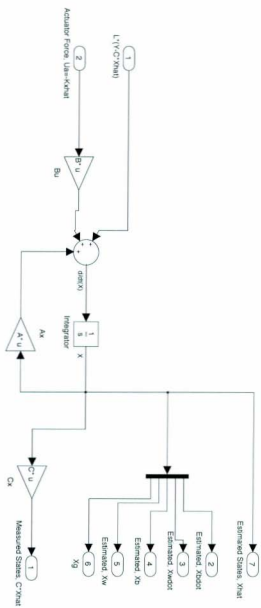


Figure D.3: State observer submodel (Kalman Observer)

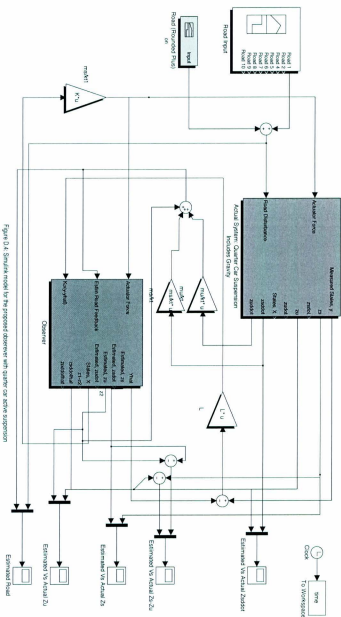


Figure D.4 Simulink model for the proposed observer with quarter car active suspension



